Sustainable Economy Research Group (S.E.R.G.)
@ CentraleSupélec Paris-Saclay University
Industrial Engineering Department (LGI)

https://www.serg.paris/

WORKING PAPER SERIES N°1

«Nuclear Cogeneration in District Heating Systems: Optimal Pathways to Decarbonization »

by

Cyrian Hallermeyer, Caroline Bono, Pascal Da Costa,
Frédéric Lantz, André Nekrasov

11-2025 WP

Nuclear Cogeneration in District Heating Systems: Optimal Pathways to Decarbonization

February 2025

Cyrian Hallermeyer[1,2,3], Caroline Bono[3], Pascal Da Costa[1], Frédéric Lantz[2], André Nekrasov[3]
[1] SERG, LGI CentraleSupélec
[2] IFPEN
[3] EDF R&D

Abstract

The decarbonization of the space-heating sector is a critical element in the global effort to transition to low-carbon energy systems. District heating (DH) systems are recognized as an effective way to combine low-carbon sources to provide heat for residential and tertiary sector buildings. As a proven technology for decarbonized electricity generation and with experience in coupling with DH networks, the use of nuclear plants in cogeneration mode to produce both heat and electricity appears to be a promising technology to contribute to the low-carbon mix for space heating. However, considering the substantial investment required for this technology and the availability of alternative low-carbon sources, such as biomass and large-scale heat pumps, the role of nuclear cogeneration in DH systems must be critically evaluated.

This paper aims to identify key factors influencing the optimal transition pathways to low-carbon DH systems with the potential to include nuclear cogeneration plants. We assess the cost-benefit analysis of nuclear cogeneration in a local context compared to alternative low-carbon heat production technologies. This paper contributes to the literature on the use of nuclear cogeneration for district heating by conducting a comprehensive study of economic scenarios for multi-year optimal decarbonization of district heating networks, and includes heat transport aspects in the modeling and economic evaluation.

Our results suggest that integrating a nuclear cogeneration plant (NCP) into the set of technologies available to the DH network brings significant system cost gains (between 2.5% and 32.3% in the configurations studied). These gains depend on the local configuration, with larger networks benefiting the most from the NCP availability. In all scenarios, investment is realized in some nuclear heat transport infrastructure, with the NCP providing the major part of the annual heat demand after 2050. Distance also influences these results, with NCPs bringing more economic benefit to the district heating network in the case of less distant installations. By studying the least-cost decarbonization pathways starting from different initial heat production mixes, we show that the investment temporality, GHG emission trajectories as well as the system cost gains brought by the NCP integration are influenced in some way by the initial heat production capacities. Limits and uncertainties of this study are also discussed.

1 Introduction

Climate change is one of the biggest challenges humanity is currently facing. In 2023, the energy sector accounted for 70% of the global greenhouse gas emissions (IEA, 2023a), due to energy systems still relying heavily on fossil fuel combustion - which account for around 80% of global energy production (2023d). To bring greenhouse gas emissions to net-zero levels, it is therefore key to transition to low carbon energy sources. At the same time, global energy consumption is expected to rise[1], driven mainly by population growth and economic development (IEA, 2023d). In 2023, approximately half of this energy was utilized for heating purposes, including industrial processes, space heating, and water heating (2023c).

In particular, the space-heating sector still has a significant journey ahead to reduce its emissions to sustainable levels. As of 2023, 63% of the energy used for building-related heating globally is still generated from the combustion of fossil fuels (2023b). In Europe, fossil fuel-based space heating accounts for a substantial share of total space-heating related consumption[2], while space and water heating as a whole represents approximately 80% of residential energy consumption in Europe (Hirsch et al., 2018). In France, for instance despite having a relatively decarbonized electricity mix and a well-electrified space-heating sector, around half of the heat consumed for space heating was still produced from fossil fuel combustion in 2021 (RTE & ADEME, 2021).

Nuclear power plants (NPP) have demonstrated their capacity to provide cost-effective low-carbon electricity, and have a role to play in the transition to zero-carbon electricity generation as large-scale zero-emission technology alongside renewable energy sources (IPCC, 2022). In addition, NPPs have shown potential to contribute not only to decarbonized electricity generation, but also to heat production for district heating (DH) systems (NEA & OECD, 2022)(IAEA, 2017). In 2015, 67 nuclear reactors were partially dedicated to non-electric purposes, of which 43 contributed to the provision of heat for DH networks. (2019). Examples of nuclear reactors operating in cogeneration mode for DH purposes can be found mainly in China, Russia, Switzerland, Slovakia (2017). Overall, the global experience in nuclear cogeneration for DH amounts to over 500 reactor years (2000).

In addition to its potential to produce decarbonized heat, the use of nuclear energy for district heating offers several other advantages highlighted in the literature. These include reducing reliance on imported fossil fuels and mitigating exposure to fossil fuel price volatility (Leurent et al., 2017)(NEA & OECD, 2022). Nuclear cogeneration could also provide consistent and stable heat production while enhancing the flexibility of electricity generation by leveraging the flexibility of DH systems (Rämä et al., 2020)(Vandermeulen et al., 2018). This approach can also help maintain reactor revenues and economic efficiency during periods when electricity production must be reduced (Locatelli et al., 2017)(Dong et al., 2021). Other studies also point out that DH systems can be built and expanded incrementally, allowing costs to be spread over time - a critical factor for large-scale projects such as coupling nuclear and DH systems (IAEA, 2017). Finally, recent advances in the efficiency of heat transport pipes have significantly reduced thermal losses, improving the overall efficiency of potential nuclear-DH systems when heat has to be transported over long distances (El Mrabet et al., 2024). Nonetheless, the economic competitiveness of nuclear energy in comparison to alternative low-carbon technologies in the context of district heating remains an important consideration. A rigorous evaluation of this competitiveness is crucial for determining the most efficient transition pathway to low-carbon heat production for DH systems.

The interest of nuclear cogeneration for DH systems depends strongly on the site-specific constraints and the macroeconomic situation at the time and place of the district heating upgrading project (Lipka & Rajewski, 2020). Therefore, rather than studying a specific project, the objective of this paper is to explore how the role of nuclear cogeneration in the decarbonization of district heating networks varies with main sensitive economic and technical factors. Among others, we wish to quantify the influence of energy and CO_2 prices, distance of heat transport, building energy efficiency evolution, and initial heat production capacities. We build a capacity expansion model for heat production and transport, and construct several scenarios (combining site-specific configurations and prospective features scenarios) to assess the impact of the parameters mentioned above on the optimal district heating network transition to low-carbon heat, and analyze if and how nuclear cogeneration fit into these scenarios. We address three research questions:

1. What additional system gains and costs does the inclusion of nuclear cogeneration bring in the transition to low-carbon heating compared to conventional-only configurations?
2. How complementary are conventional heat sources and nuclear cogeneration in an optimal trajectory of district heating networks to zero emissions?
3. How are the results to the two questions above influenced by major sensitive economic and technical parameters ?

To address these questions, we adopt the perspective of a benevolent social planner realizing the investment and operation decisions for a district heating network. For the planner, the use of heat supplied by a nuclear cogeneration is an option in competition against more conventional heat sources, such as gas boilers, biomass burners or heat pumps. We develop a Mixed-Integer Linear Programming model to represent our Generation Expansion Planning problem. The investment and operation decisions are realized over 40 years, from 2025 to 2065, as we are interested in getting the optimal pathways to reach zero emissions goals for the district heating network. We analyze the outcomes of our model on the several scenarios built in terms of total cost system, installed capacities, heat load dispatch, emissions trajectories, and marginal heat cost realization. The scenarios assessed combine prospective parameter variations (e.g. electricity prices, heat demand evolution) and site-specific requirements (e.g. distance of heat transport, size of the DH network).

Our results suggest that integrating an NCP into the set of technologies available to the DH network brings significant system cost gains, as well as important economic benefits to the NCP operator in all studied configurations and scenarios. These gains depend on the local configuration, with larger networks benefiting the most from the NCP availability. In all scenarios, investment is realized in some nuclear heat transport infrastructure, with the NCP providing at the major part of the annual heat demand after 2050. The distance and initial heat production mix also influence these results.

The paper makes three key contributions to the literature. We build a multi-year framework of investment-operation decisions for a district heating network with the possibility to use nuclear cogeneration. In addition, we include nuclear heat transport infrastructure economic and technical parameters and limitations into the modelling framework. Finally, we build multiple local configuration and

[1] Although it is decreasing in Europe, and expected to remain stable in OECD countries in general (Energy Information Administration - EIA, 2021).

[2] Around 60% in 2022 (Eurostat, 2022)

prospective features scenarios to quantify the impact of macroeconomic and site-specific factors on the optimal pathways to DH decarbonization.

The rest of the paper is organized as follows: Section 2 provides an overview of existing studies on the coupling of nuclear cogeneration with district heating networks, Section 3 describes the modeling methodology employed. Section 4 presents our results and discusses their main implications. Section 5 concludes and provide suggestions for refinement of this work.

2 Background

The increasing interest in the use of nuclear to decarbonize DH reflects in the growing literature on the subject. First, several studies have explored the benefits of integrating non-electrical applications with nuclear reactors to improve load following capabilities. These studies specifically focus on the reactor side of the hybrid system. Locatelli et al., 2017 assess the techno-economic feasibility of combining cogeneration systems, such as district heating and desalination, with NPPs. The study finds that cogeneration effectively utilizes excess power, enhancing operational flexibility while remaining economically viable.

Other studies propose an analysis of NCPs from an energetic and exergetic efficiency point of view. Safa, 2012 examines the use of superheated steam from NPPs for district heating, and underlines improvements in heat piping insulation that allow for efficient heat transport over long distances. The study employs thermodynamic analysis on a modified Rankine cycle to show that a significant portion of wasted heat could be recovered and utilized in urban heating systems. Xu et al., 2021 have also investigated the coupling of a cogeneration SMR with a district heating system from an energetic and exergetic efficiency analysis. They conclude that the coupling of a 35MW$_{th}$ SMLFR[3] with DH can reach a 73% energy efficiency and a 59% exergetic efficiency with optimized DH and SMR designs and operation. As a general conclusion, they emphasize that optimizing the heat extraction system features (temperatures, flows, tapping points) in the secondary circuit, as well as the exchange with the district heating system is key to improve thermodynamic efficiency. Other studies have explored the use of thermal energy storage (TES) in a coupling scheme with hybrid nuclear reactors, from the perspective of thermal efficiency optimization. Edwards et al., 2016 investigate the integration of thermal energy storage with nuclear power plants, focusing on methods like exergy analysis and energy density modeling to evaluate storage media such as molten salts and synthetic heat transfer fluids. The study finds that these options vary in effectiveness, with synthetic fluids performing well with light-water reactors and liquid salts better suited for advanced reactors. Hadi Ghazaie et al., 2022 conduct the techno-economic assessment for a SMLFR coupled with latent heat storage to hourly meet an exogenous heat load. They conclude that the coupling of the SMR and the TES could meet the flexibility requirements from the thermodynamics viewpoint, and reach close to 75% thermal efficiency.

Moreover, some studies have emphasized the importance of considering heat transport systems in the modeling of hybrid nuclear systems, as they account for a significant portion of the total cost of such systems (Leurent, Da Costa, Jasserand, et al., 2018). Hirsch et al., 2018 introduce a Decision Support System (DSS) designed to optimize the design and operation of long-distance heat transport systems. The DSS incorporates factors such as system life cycle, heat demand variability, and terrain elevation. Key parameters like pipe diameter, insulation thickness, and pumping station locations are optimized using a genetic algorithm to minimize construction and operating costs while reducing heat loss. Li et al., 2019 present a combined heat and water (CHW) system designed for long-distance heat transport, using water from the supply system as a heat carrier. The study employs a detailed model to analyze the system's efficiency, revealing that it can transport heat over distances exceeding 200 km with significant cost and efficiency advantages compared to traditional methods. Chen et al., 2021 apply a CHW system to the Jiaodong Peninsula, using four AP1000 units to address local heat and water shortages. The study highlights the system's effectiveness in meeting 38% of the heat and 72% of the water demand, and emphasizes its social, environmental, and economic benefits. Leurent, Da Costa, Jasserand, et al., 2018 compare various low-carbon heating systems for Lyon, including large-scale heat pumps and a nuclear combined heat and power plant (NCHP). The analysis finds that an NCHP located about 30 km from Lyon offers the best balance between CO_2 emissions and heating costs, providing valuable insights for similar metropolitan areas.

Several papers have explored the modeling of complex heat production mixes for DH systems and the integration of NCPs along other technologies. A. Gabbar et al., 2020 compare five different hybrid energy systems, including mixes of fossil-based thermal plants, renewable electricity sources, and a micro-modular reactor (MMR). The dispatch of the different units is based on a fixed decision scheme described in the paper. The electricity produced by local units is used in priority to meet the local load, then the battery can provide the additional power needed, then diesel generators, and in last resort the grid can be used (for allowed cases). They conclude that the Nuclear-Renewable hybrid system was the one achieving the lowest emissions while minimizing the cost of energy, compared to cases where renewables where coupled to fossil-fuel CHP units. Rämä et al., 2020 explore a flexible nuclear co-generation concept where plants adjust heat and electricity output using steam at different pressure levels, integrated with district heating and large-scale heat storage. The authors frame their simulation as a Mixed-Integer Linear Programming (MILP) optimization model to assess the concept's efficiency in three French cities—Paris, Lyon, and Dunkirk. Lindroos et al., 2019 investigate the integration of SMRs with heat pumps and heat-only boilers to supply heating and cooling for a district heating and cooling (DH/DC) network, particularly in the context of decommissioning coal plants. The study examines two scenarios: using an SMR in heat-only mode (DHR-400) and employing a cogeneration approach with a NuScale-type reactor. The authors formulate their problem as an operation model run several times with multiple input investment decisions. Liu et al., 2023 considered a DHR-400 working in heat boiler mode exclusively, coupled to a district heating load, accompanied by a TES and a gas boiler to meet the hourly load. The dispatch strategy is based on fixed rules: giving priority to the DHR-400, followed by the thermal storage, and the gas boiler in last option. An MINLP is run to optimized the installed capacities of TES and peak gas boiler. Värri and Syri, 2019 compare the economic benefits of adding a cogeneration SMR (based on NuScale[4] features) to heat production mix of Helsinki metropolitan area. The hourly dispatch is done with a merit order model, and the investment decision model works

[3] Small Modular Lead-cooled Fast Reactor

[4] See IAEA. "NuScale Power Modular and Scalable Reactor"; IAEA: Vienna, Austria, 2013.

from full load hours scenarios to compute optimal capacities for each technologies. They use their dispatch-investment combined model on different scenarios of SMR penetration, and conclude that under their median scenario assumptions, it is profitable for the local system to add a cogeneration SMR. Pursiheimo et al., 2022 explore the decarbonization of the district heating and cooling (DHC) system in the Helsinki metropolitan area by simultaneously evaluating the integration of heat pumps, gas and biomass boilers and SMRs. The study formulates an MILP optimization problem to analyze the projected 2030 situation, considering various scenarios with different assumptions about the existing DHC system, investment costs, and electricity prices. Finally, Abushamah et al., 2023 optimize the investment and operation of SMRs to supply heat for a DC network (running on absorption and compression chillers, along with storage). They propose a linearization of non-linear equations governing heat transport to make the problem solvable in a reasonable time. Their model, which includes a one-year simulation, integrates both the investment and operational aspects of both the nuclear units and the heat transport system between the reactors and the DC network.

Existing studies in the integration of nuclear cogeneration in district heat production generally exhibits one or several of the following attributes: They may ignore the heat transportation system by only considering configurations where the NCP is closeby the DH network. They only consider one-year simulations to make the operation and investment decisions on the DH system. They consider fixed-dispatch rules and technology-by-technology cost-assessments rather than an optimal decarbonized heat production mix. Our contribution to the literature is threefold. We consider a multi-year framework of investment-operation decisions, including nuclear heat transport infrastructure investment and operation cost, and build multiple local configuration and prospective features scenarios to quantify the impact of macroeconomic and site-specific factors on the optimal pathways to DH decarbonization.

3 Methodological framework and modeling

In this section, we detail the modeling methodology chosen to represent the coupling of an NCP with a DH network. We model the use of an NCP to provide both heat for a DH network, and electricity to the grid. The NCP model and parameters are based on the Pressurized Water Reactor (PWR) technology, which is the most common technology of nuclear reactors currently in operation in the world[5]. The DH network is connected to several heat production capacities, including the NCP, and the dispatch of the heat load among the different plants is done on an hourly basis. The setup of the study if represented on Figure 1. We adopt a Generation Expansion Planning approach to our problem, by minimizing the total cost of the system, while meeting the heat demand of the DH network. The methodology section is organized in three sub-sections. Sub-section 3.1 provides a general description of the model, and a presentation of the main sub-systems modeling assumptions. As we are interested in quantifying the impact of local configurations and macro economic parameters on the role nuclear cogeneration can play in decarbonizing DH networks, we develop several scenarios of local configurations and prospective economic inputs. These scenarios are detailed in 3.2. Moreover, as we wish to simulate the evolution of investments in production and transport capacities over the years, as well as the hourly dispatch of the heat load among the different plants. However, running the optimization model with an hourly time resolution over multiple years is computationally expensive. Therefore, we adopt a temporal aggregation resolution, that is detailed in Section 3.3. Finally, sub-section 3.4 describes the main equations of the model and is structured by sub-system. Notations, decision variables, and main parameters are discussed in this section.

3.1 Model description

The model is composed of four main sub-systems: a DH network receiving heat from heat production capacities, a nuclear cogeneration plant (NCP) producing heat and electricity, a heat transmission network (HTN) to transport heat from the NCP to the DH (distribution) network, and alternative heat production capacities (AHPC) also producing heat for the DH network. These sub-systems are represented on Figures 1 and 2. The modeling horizon is 2025 to 2065, with nuclear capacities being only available starting 2035.

In the secondary circuit of the NCP, the Balance of Plant (BoP) operates the dispatch of the steam obtained from the steam generator between the conventional island, which produces the electricity, and the heat extraction system. This module corresponds to the upgrade from a pure power generation NPP to an NCP, and includes the heat exchangers allowing heat to be transferred to the HTN. The latter consists of a supply circuit and a return circuit, each of them composed of parallel pipes. The NCP can provide electricity to the grid, for which it is assumed to be a price taker [6], and heat via the HTN to the DH network. The HTN, which is composed of supply and return pipes, and supply and return pumping stations, transports heat in the form of super-heated water. The modeling of the DH network itself is out of the scope of this paper. We represent it as a heat sink with a perfectly known exogeneous load demand and temperature requirement. Finally, we assume the AHPCs to be located much closer to the DH network than is the NCP. Therefore the transmission networks from the AHPCs to the DH network are not included in the model.

The AHPCs are subject to technical constraints that are detailed in sub-section 3.4.5 along with the detail of their cost, including installation costs, operation costs, and the price of CO_2 emissions for plants that rely on fossil fuel combustion. The installation and use of AHPCs can be restricted by resource availability constraints, for example in the case of geothermal pumps, or solid biomass boilers. Finally, the total annual CO_2 emissions of the system is restricted by an annual cap, decreasing with years.

3.2 Data and scenarios calibration

In order to quantify the impact of different economic parameters on the interest of nuclear cogeneration to supply heat to a DH network, we design several scenarios of input parameters and run the optimization model for each of them. We study the impact of five main parameters on the optimization results: The initial heat production mix, the initial annual heat demand, the distance between the NCP and the DH network, the electricity prices, and annual heat demand evolution. The three first parameters constitute a set of local configurations, which correspond to the specificities of local situations in

[5] See (IAEA, 2020).

[6] This assumption is consistent with assumptions made by multiple studies on nuclear cogeneration plants coupling with DH networks, including Leurent, Da Costa, Jasserand, et al., 2018, Rämä et al., 2020, and Pursiheimo et al., 2022

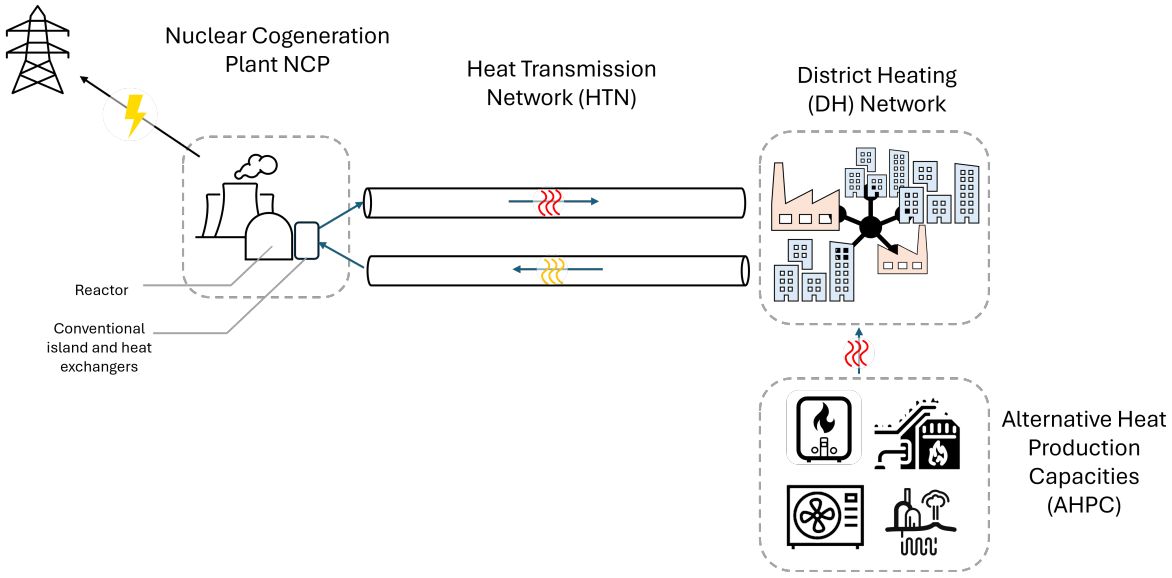

Figure 1: General setup of the study

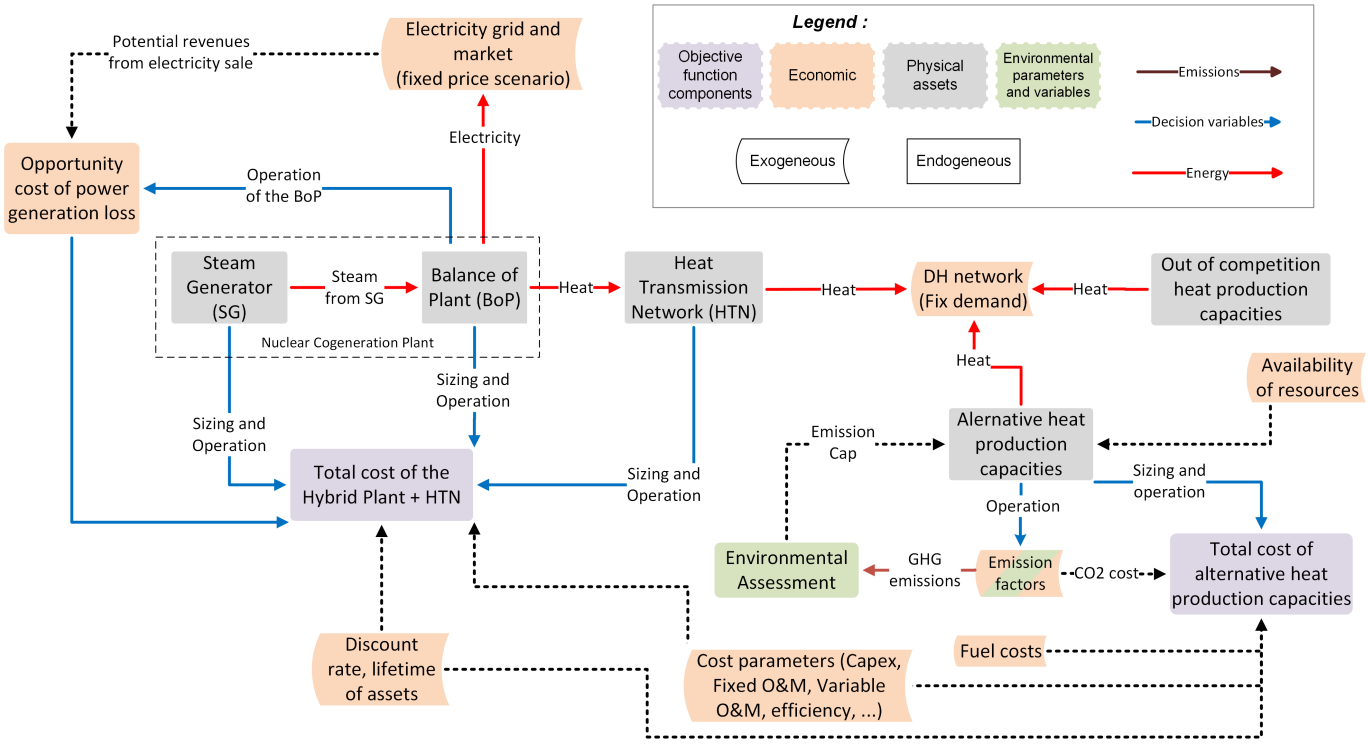

Figure 2: Model sub-components

which nuclear cogeneration coupling with DH networks can happen (Section 3.2.1). The electricity prices and annual heat demand evolution correspond to prospective data, for which the inherent uncertainty justify to split our analysis in four prospective scenario (Section 3.2.2).

3.2.1 Local configurations details

Initial annual heat demand. We choose to model two sizes of DH network: 0.5TWh and 5TWh annual consumptions. To provide orders of magnitude, 1TWh corresponds to approximately 70,000 homes if we consider the average energy consumption for space-heating in Europe (Odyssee-Mure, 2020). A 0.5TWh/a DH network corresponds to the DH network of Lyon. A 5TWh/a consumption corresponds to the one of the current Helsinki DH network. The shape for the hourly heat demand pattern is the same accross all scenarios, and we assume that this shape remains the same throughout the years. We detail in Appendix 6.2 how this shape is determined. The heat demand is exogenous, assumed fully inelastic to heat costs.

Initial capacities scenarios Since we study the evolution of DH production mix over multiple decades, the initial state of the heat production mix has an influence on the results in terms of newly installed capacity, heat production dispatch, GHG emissions, and in total cost of the system. We build two synthetic configurations representing the diversity of heat production mixes.

Our first configuration (referred as Geo) is inspired from the Helsinki metropolitan area case (studied in (Pursiheimo et al., 2022) and (Lindroos et al., 2019) for instance). We gathered data from the Helsinki Region Environmental Services Authority[7], providing the heat produced by technology from 2000 to 2023. We replaced coal and oil based heat production by a mix of biomass, heat pumps, and natural gas boilers. Heat pumps used in Helsinki DH are for most of them fatal heat recuperation heat pumps, data-center based heat pumps, or geothermal heat pumps, with efficiencies ranging between 300% and 500%. We assume that they can all be gathered in one category, geothermal heat pumps, with efficiency of 350%.

The second synthetic configuration (referred as Bio) is inspired from Kaunas DH, whose heat production mix is described in (Hast et al., 2018). Kaunas is the second largest DH newtork in Lithuania, with an annual consumption of 1TWh. Solid waste incineration provides about a tenth of heat supply, biomass about half, and natural gas provides the rest.

We adjust our two synthetic cases to make them comparable in terms of decarbonization efforts. We scale solid waste incineration to 10% of the initial annual heat consumption and natural gas boilers (NG) to one third of it. Table 1 summarises the composition of the initial mix of our two scenarios. We obtained the initial capacities by backward solving the dispatch merit-order, assuming capacities are dispatched in the following order: *Solid Waste Incineration (SWI)* → *Geothermal* → *Solid Biomass* → *NG*

Table 1: Scenarios of initial capacities

2025 consumption	Mix type	Initial capacities (MW)				
		NG	Biomass	SWI	Geothermal	HP
0.5TWh	Geo	118.49	10.25	5.71	34.89	0
	Bio	118.49	45.14	5.71	0	0
5TWh	Geo	1184.9	102.5	57.1	348.9	0
	Bio	1184.9	451.4	57.1	0	0

The interest of the Bio mix is that it allows to study the effect of nuclear cogeneration integration into a mix whose cost is less dependent on electricity prices. In the Geo mix, the inital heat production capacities rely of two almost third (in terms of heat produced) on capacities consuming electricity. Since the cost of heat production from the NCP includes an opportunity cost due to the loss of electricity production, it depends on the electricity prices at which this lost electricity could otherwise be sold. Therefore, it is of interest to understand whether the dependence of the rest of the mix on electricity prices affects the results of the optimization model.

These scenarios rely on resources with limited potential for exploitation, namely solid biomass, geothermal energy and solid waste. First, we enforce that the model cannot install these technologies if they are not initially present. Secondly, we assume that the resources in biomass will remain constant throughout the years. For the case including geothermal capacities, we also assume that its potential can be extended twofold (based on prospective data for the Helsinki area from (Pursiheimo et al., 2022)). For SWI, we assume that the potential of heat recovery from waste incineration in these DH networks is already exploited at its maximum. Finally, the model can install heat pumps capacities without limitation, but NG boilers can only be decommissioned. Technical and economic parameters used for AHPCs are summarized in tables 8, 2 and 9.

Distance between the NCP and the DH network As suggested in several papers, see for example (Leurent, Da Costa, Rämä, et al., 2018) or (Hirsch et al., 2018), there are significant costs associated with transporting heat over long distances due to pressure drop compensation, heat losses and infrastructure costs for kilometres of piping. Therefore, we believe it is essential to evaluate our framework over a wide range of heat transport distances to understand how the influence of economic and technical parameters varies with transport distance.

(Leurent, Da Costa, Rämä, et al., 2018) summarized the interest expressed by several entities for nuclear cogeneration applied to district heating for specific urban areas, and the associated length of heat transport lines. Based on there results, we choose to retain distances of 20 and 40 kilometers for our study. Pipes available to the model have repsective diameters of 300, 500, 600 and 1000 millimeters. More details on the pipes characteristics are provided in Appendix 6.6.3.

Combined with the two initial capacity configurations Geo and Bio, this results in four local configurations: Geo20, Geo40, Bio20, and Bio40. Moreover, reference (baseline) configurations Geo and Bio for which nuclear cogeneration is not available are referred to as **Geo∅** and **Bio∅**. These last two scenarios will serve as a reference to quantify the impact of nuclear cogeneration availability on decarbonization costs and on the investment and operation of heat production capacities.

3.2.2 Prospective data scenarios

Electricity prices The trade-off between electricity and heat production by the NCP depends on the price at which electricity can be sold by the plant to the grid. We therefore want to test our framework for various electricity price scenarios.

There are two parameters of interest for the electricity price curves: the average annual price level and the volatility. We use these two parameters to construct two scenarios of electricity prices: a low price scenario and a high price scenario. The data used in calibrating our model are based on hourly and seasonal deformation factors calculated based on the EU-Sysflex European project scenarios. The construction of these scenarios and the hourly shape of the electricity prices is detailed in the appendix 6.4. The characteristics of the scenarios are summarized in table 10.

Interannual heat demand trends In terms of annual demand evolution, the annual demand is assumed to be constant after 2050 in all scenarios, but follows different trends between 2025 and 2050. To account for the dual effect of efficiency gains[8] and energy service demand reduction, we define a demand scenario where the annual demand decreases by 1% every year[9] between 2025 and 2050. On the other end, we also consider a scenario where heat demand increases by 0.9% every year due to the expansion of the DH network to new buildings, and to possible reduced building

[7] See https://www.hsy.fi/en/environmental-information/open-data/avoin-data---sivut/district-heating-in-the-helsinki-metropolitan-area/

[8] Renovation or replacement of old buildings for example.

[9] We choose these numbers based on the scenarios of the report of the European project "Hotmaps - Heating and Cooling Open Source Tool for Mapping and Planning of Energy Systems" (Hotmaps Project, 2021) which forecast final energy demand provided by DH to decrease in EU28 from 350TWh to 250TWh between 2030 and 2050.

renovation efforts.

Combining the low and high electricity price variants with the increasing and decreasing heat demand scenarios results in four prospective scenarios, hereafter referred to as *Favored Expansion* (*Fav.Expan*) (increasing demand, low electricity prices), *Chosen Expansion* (*Ch.Expan*) (increasing demand, high electricity prices), *Chosen Efficiency* (*Ch.Effi*) (decreasing demand, low electricity prices), and *Constrained Efficiency* (*Con.Effi*) (decreasing demand, high electricity prices). These prospective senarios are summarized in Figure 3.

The *Favored Expansion* scenario corresponds to a context of continued expansion of the heat demand, correlated with relatively low electricity prices. The low electricity prices drive heat prices down since part of the demand can be met by electric means. These low prices encourage less effort to renovate buildings and less intensives to curb heat consumption. The *Chosen Expansion* scenario corresponds to a continuing expansion of the heat demand, despite relatively high electricity prices (and hence relatively high heat prices). This second scenario represents a context where high energy prices do not lead to energy efficiency and energy conservation measures. The *Chosen Efficiency* scenario correspond to context of decreasing heat demand, despite low electricity prices. This corresponds to strong building renovation policies and voluntary heat consumption reduction. Finally the *Constrained Efficiency* scenario correspond to context of decreasing heat demand due to high electricity prices. This scenario represents a context where high electricity prices produce high heat prices, and therefore encourages energy efficiency measures and a reduction of domestic heat consumption.

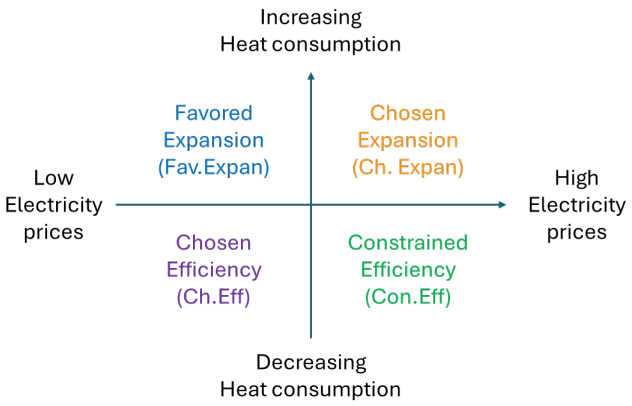

Figure 3: Prospective Scenarios

3.2.3 Other exogenous parameters calibration

CO_2 emissions annual cap and price The CO_2 emissions annual cap applied to all scenarios must make them comparable. Therefore, we calculate this cap for each scenario based on a common decreasing heat-GHG intensity parameter. The initial GHG intensity of heat in all scenarios is equal to $89 gCO_2eq/kWh$, so we choose this value as our 2025 GHG intensity cap. Thereafter, the annual GHG intensity cap is decreasing linearly to reach zero in 2050.

In order to account for additional costs incured by heat sources emitting greenhouse gases, we add an exogenous CO_2 price to the gas price assumed for gas boilers variable operation cost. This exogenous CO_2 price is used as a proxy to represent the impact of emission trading systems (EU-ETS for instance) or carbon taxes that may be implemented at the national and/or continental level. In this paper, we assume that the CO_2 price rises linearly from 100€/tCO_2eq in 2025 to 200€/tCO_2eq in 2050.[10] These are conservative asumptions since these values are much lower than the tutelary CO_2 values proposed in (Quinet et al., 2019) whose results indicate that a tutelary value of around $270€_{2025}/tCO_2$ in 2030 and $1300€_{2025}/tCO_2$ in 2045 would be necessary to reach the net-zero target. However, since we enforce an emission cap on the local system, we only wish to represent a proxy of the additional cost to which gas burners capacities are subject due to national GHG taxation or emission trading systems.

Fuel prices Consistant with fuel price data from (Pursiheimo et al., 2022), gas prices are assumed to increase linearly from 40€/MWh in 2025 to 70€/MWh 2050 and remains stable after 2050. Similarly, we assume biomass to increase linearly from 30€/MWh to 50€/MWh. Sensitivity analysis will be conducted on these parameters.

Table 2: Fuel cost parameters

Parameter	Value (€/MWh)	Source
Electricity price	See prospective scenarios	-
Solid Wastes	0€/MWh	-
Gas price	40 → 70€/MWh until 2050, stable after	(a)(b)
Biomass price	30 → 50€/MWh until 2050, stable after	(a)(c)
CO_2 price	100 → 200€/MWh until 2050, stable after	(d)(e)

(a) (2022), (b) (Carlsson et al., 2012), (c) (Lindroos et al., 2019), (d) (Enerdata, 2023)

3.3 Temporal aggregation resolution

The computational challenges arising from the integration of short-term operations with long-term energy system planning have been recognized in several studies, which highlight the need for modeling strategies to ensure that problem-solving remains feasible within a reasonable time (Helistö, Kiviluoma, Holttinen, et al., 2019)(Fehrenbach et al., 2014). In order to reduce the computational complexity of the optimization problem, we propose to use a temporal aggregation resolution[11] that relies on the use of representative weeks to model the short-term operation of the NCP, the HTN and the AHPCs. Our approached is illustrated on Figure 4. We first run the model in investment mode, where the model is free to invest in capacity according to the rules described later in this section. Investment decisions are saved and used as it in the operation phase.

The model time horizon spans over $N = 40$ years, from 2025 to 2065, and is divided in year blocks $\{[y_n, y_{n+1}[, n \in [\![1, N]\!]\}$, of a length of 5 years. In the investment phase, the model can invest in new AHPCs (when allowed), in new pipes and pumping capacities for the HTN, and in additional capacities for the heat extraction system, at the beginning of each year block. The model can also decommission some of these infrastructures at the beginning of each year block. The construction and decommissioning times are assumed to be zero (assuming anticipation from the planner). Each year block is then divided in several representative weeks. Within each representative week, the load dispatch among the heat production capacities, the NCP dispatch between electricity and

[10] The price after 2050 has no importance here since the decarbonization constraint enforced in the model implies no CO_2 emissions after 2050.

[11] See (van der Heijde et al., 2018) and (Helistö, Kiviluoma, Ikäheimo, et al., 2019) for examples of studies on district heating dispatch employing temporal aggregation in representative periods.

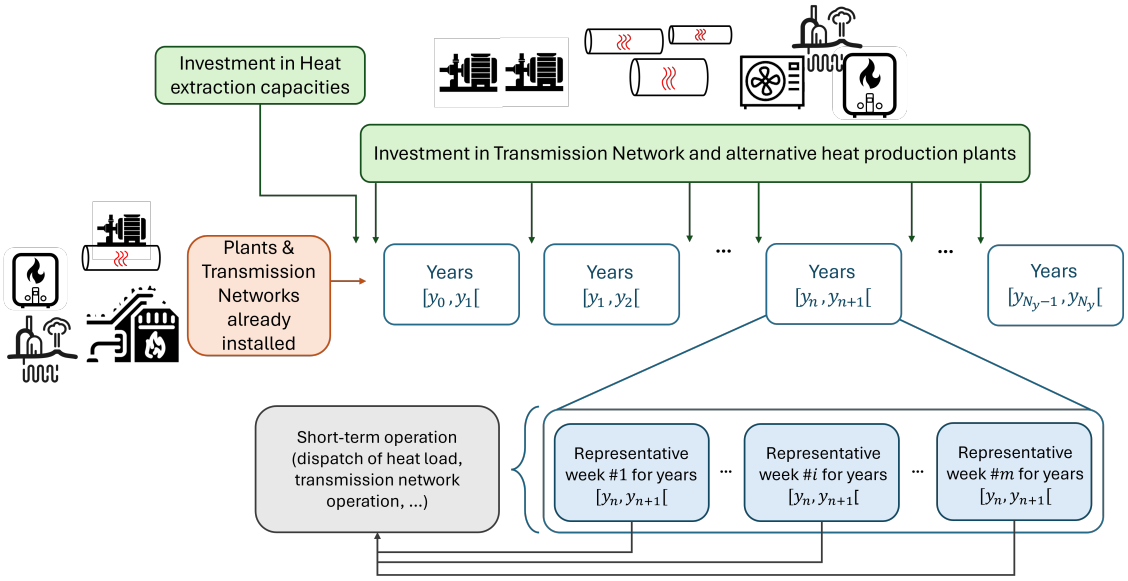

Figure 4: Investment options and operation loops in the optimization model

heat, and the HTN operating conditions are solved with and hourly resolution, similar to the operation phase. As documented in (Helistö et al., 2020) several methods exist to perform a representative weeks selection. Based on their conclusions on the effectiveness of a K-means-based sampling method to generate representative week producing accurate results in GEP problems, we adapt a K-means clustering algorithm to our needs, the details of which are presented in Appendix 6.5: For each year block, we select the week with the peak demand, plus 7 other representative weeks. For each year block, a K-means custering is applied (with 7 clusters) with the electricity price and heat demand data as input data. For each cluster, we keep the week with the Euclidian distance to the other cluster samples data.

3.4 Model equations

3.4.1 Notations

The notations used in the model are introduced when needed throughout the paper, and summarized in tables 6 and 7 in Appendix 6.1. For clarity, we detail here the main notations used in the following sections. Alternative heat production capacities are indexed by $k \in \mathscr{K}$. Year blocks are indexed by $y \in \mathscr{Y}$ (year block y_n corresponds to the years in interval $[y_n, y_{n+1}[$), and hours are indexed by t. Pipes of the HTN are indexed by $i \in \mathscr{I}$, and the pipe combinations are indexed by $j \in \mathscr{J}$ (the link between pipes and pipes combinations is detailed in Section 3.4.4). The decisions variables of the model are the following:

- $K^{capa,new}_{k,y}$ [MW]: capacity of AHPC k added or decommisioned at the beginning of year block y.
- $\mathbf{I}^{pipe}_{i,y}$: indicator function of pipe i being built at the beginning of year block y.
- K^{ext} [MW]: capacity of the heat extraction system.
- $K^{pump,new}_{y}$ [MW]: pumping power capacity added or decommissioned at the beginning of year block y.
- $q^{capa}_{k,t}$ [MWh]: hourly heat production of alternative heat production capacity k.
- q^{supp}_{t} [MWh]: hourly quantity of heat supplied by the NCP to the DH network through the HTN.
- $\mathbf{U}^{comb}_{j,t}$: indicator function of pipe combination j being used at time t.

3.4.2 Objective function and production-demand adequacy

The objective function of the optimization problem, given in Equations (1) and (2), is the discounted total cost of the system over the simulation horizon. It includes installation costs of new infrastructures (for the heat extraction system, for the HTN, and for the AHPCs), fixed operation and maintenance (FOM) costs for heat extraction, production capacities, pipes, and pumping capacities, and variable operation costs for heat production, nuclear heat extraction, heat transport, and pumping capacities. Coefficient $\beta = \frac{1}{(1+r)}$ is the discount factor, with r the discount rate.[12]

$$Obj = \sum_{y \in \mathscr{Y}} \beta^y Obj_y \tag{1}$$

with

$$\begin{aligned} Obj_y = {} & IC^{ext}_y + IC^{pump}_y + \sum_{i \in \mathscr{I}} IC^{pipe}_{i,y} + \sum_{k \in \mathscr{K}} IC^{capa}_{k,y} \\ & + FOM^{ext}_y + FOM^{pump}_y + \sum_{i \in \mathscr{I}} FOM^{pipe}_{i,y} + \sum_{k \in \mathscr{K}} FOM^{capa}_{k,y} \\ & + \sum_{y \in \mathscr{Y}, t' \in \mathscr{T}_y} (VO^{ext}_{t'} + OC_{t'} + VO^{pump}_{t'} + \sum_{k \in \mathscr{K}} VO^{capa}_{k,t'}) \end{aligned} \tag{2}$$

Equation (3) enforces the adequacy between heat supply from the NCP (q^{supp}) and AHPCS (q^{capa}), and net heat demand from the DH network (q^{dem}). Heat losses in the transmission pipes are accounted for in the calculation of q^{supp}.

[12] r is set to 3% in this paper, in accordance with (European Commission, 2014)

$$q_{t'}^{dem} = q_{t'}^{supp} + \sum_{k \in \mathcal{K}} q_{k,t'}^{capa} \tag{3}$$

Cap on GHG intensity of produced heat is enforced at every year in Equation (4).

$$\sum_{k \in \mathcal{K}} \sum_{t' \in \mathcal{T}_y} q_{k,t'}^{capa} \cdot EF_k^{capa} \leq E_y^{max} \cdot \sum_{t' \in \mathcal{T}_y} q_{t'}^{dem}, \forall y \tag{4}$$

3.4.3 Nuclear cogeneration plant

The NCP is modeled as a secondary circuit, represented on Figure 5, with two turbines connected to a steam generator. The reheating stages between the high and low pressure turbines and at the outlet of the condenser are not shown on the Figure for the sake of clarity. The secondary circuit is considered a Rankine cycle (with a superheating of the steam between the high and low pressure tubines) with nominal efficiency η_{ran}, from which the BoP can extract heat in the form of steam. We consider three possible tapping points (which can be used simultaneously) to extract steam from the secondary circuit: at the inlet of the high pressure turbine, at the outlet of the high pressure turbine and at the inlet on the condenser. The steam extracted passes through a heat exchanger to provide heat to the heat transmission network. These extraction points has been identified in different studies as a reliable source of sufficient quality steam[13]. There is a trade-off between the electric power produced by the NPP and the heat extracted, since steam extraction in the secondary circuit decreases the steam flow that passes through the stages of the high and low pressure turbine.

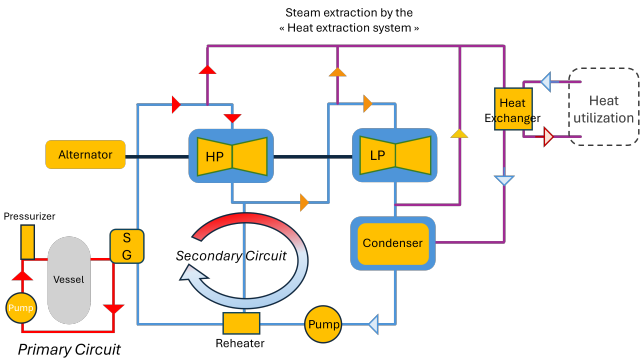

Figure 5: Secondary circuit of an NCP including steam extraction from the feedwater circuit of the high and low pressure turbines.

The equations modeling the steam extraction, its cost is terms of loss of electricity production ($\Delta P_{t'}^{e}$), and the technical limitations applying to the extraction module are provided with their explanation in Appendix 6.6.1

The installation cost of the heat extraction system (IC^{ext}), its FOM (FOM^{ext}) and its variable operation cost (VO^{ext}) are modeled with Equations (5) - (7).

$$IC_y^{ext} = c^{ext,inst} \cdot K^{ext} \tag{5}$$

$$FOM_y^{ext} = c^{ext,fom} \cdot K^{ext} \tag{6}$$

$$VO_{t'}^{ext} = c^{ext,vo} \cdot q_{t'}^{ext} \tag{7}$$

[13] See for example (ETI, 2016), (Li et al., 2019), or (Rämä et al., 2020)

The cost of the heat produced by the NCP and extracted by the heat extraction system should also include the loss of power generation. We model this cost with an opportunity cost (OC), assuming that the steam that is extracted would otherwise be used to produce electricity, and that the steam generator works at maximum rate. The installation and O&M costs of the NPP itself are not directly accounted for in our analysis, but indirectly modeled in the opportunity cost, while the additional installation and O&M costs due to the upgrading of the NPP to an NCP are accounted for in the heat extraction system cost parameters[14].

$$OC_{t'} = p_{t'}^{e} \cdot \Delta P_{t'}^{e} \tag{8}$$

3.4.4 Heat Transmission Network

The model can invest in individual pipes, but uses pipe combinations in the operation equations. Therefore Equations (9) and (10) make the conversion between the availability of pipes and availability of pipe combinations. Equations (11) and (12) enforce that a combination can only be used if it is available, and that only one combination at a time is used. $\mathbf{A}_{j,y}^{comb}$ is the indicator function of pipes combination j being available for use during year block y. M_{conv} is the conversion matrix define as: "$M_{conv}[i,j] = 1$ if pipe i is in combination j, else 0", and $N_j^{pipe} = \sum_{i \in \mathcal{I}} M_{conv}[i,j]$ the number of pipes in combination j.

$$\mathbf{A}_{j,y}^{comb} \leq \sum_{i \in \mathcal{I}} M_{conv}[i,j] \mathbf{A}_{i,y}^{pipe} / N_j^{pipe} \tag{9}$$

$$\mathbf{A}_{j,y}^{comb} \geq \sum_{i \in \mathcal{I}} M_{conv}[i,j] \mathbf{A}_{i,y}^{pipe} - N_j^{pipe} + 1 \tag{10}$$

$$\sum_{j \in \mathcal{J}} \mathbf{U}_{j,t'}^{comb} \leq 1 \tag{11}$$

$$\mathbf{U}_{j,t'}^{comb} \leq \mathbf{A}_{j,y}^{comb} \tag{12}$$

Then, Equations (13) and (14) describe the installation of pipes for the heat transmission network. Each pipe can only be built at most once, and pipes are only available for use if they have been built. The lifetime of pipes is assumed to be longer than the simulation horizon. $\mathbf{A}_{i,y}^{pipe}$ is the indicator function of pipe i being available during year block y, and $\mathbf{I}_{i,y}^{pipe}$ is the indicator function of pipe i being built at the beginning of year block y. Parameter l_{pump} corresponds to the lifetime of pumps, and $\mathbf{I}_{i}^{pipe,ini}$ is an indicator of pipe i being already installed before the beginning of the simulation horizon (in case the HTN already exists). Finally, equations (15) to (16) model the inertia of the pipes: A pipe combination cannot be used less than $t_{inertia}$ hours in a row, with $t_{inertia}$ being fixed here to 168 hours. If all pipes are turned off, they must remain off for at least $t_{inertia}$, and to simplify the computational burden, pipe combinations cannot be changed inside a day.

[14] Following the methodology described in (IAEA, 2017), the incremental costs should take into account the cost of electricity production that the NPP would incur in pure power generation operation. However, we assume that the NCP would bid into the local heat market at a price equal to the opportunity cost of not producing the equivalent amount of lost electricity, and therefore use the electricity market price in our opportunity cost formula.

$$\sum_{y \in \mathscr{Y}} \mathbf{I}_{i,y}^{pipe} \leq 1 - \mathbf{I}_{i}^{pipe,ini} \tag{13}$$

$$\mathbf{A}_{i,y}^{pipe} = \mathbf{I}_{i}^{pipe,ini} + \sum_{y' \leq y} \mathbf{I}_{i,y'}^{pipe} \tag{14}$$

$$\mathbf{U}_{j,t'}^{comb} \geq \mathbf{U}_{j,t'-1}^{comb} + \mathbf{U}_{j,t'-t_{inertia}}^{comb} - 1 \tag{15}$$

$$\sum_{j \in \mathscr{J}} \mathbf{U}_{j,t'}^{comb} \leq 1 + \sum_{j \in \mathscr{J}} \mathbf{U}_{j,t'-1}^{comb} - \sum_{j \in \mathscr{J}} \mathbf{U}_{j,t'-t_{inertia}}^{comb} \tag{16}$$

The cost of the heat transmission network is composed of the variable cost of pumping the water in the pipes ($VO_{t'}^{pump}$), the installation costs (IC_{y}^{pump} and $IC_{i,y}^{pipe}$), and of the fixed O&M costs (FOM_{y}^{pump} and FOM_{y}^{pipe}) of the pumping stations and the pipes. These costs are modeled with the following equations:

$$IC_{i,y}^{pipe} = c_{i}^{pipe,inst} \cdot \mathbf{I}_{i,y}^{pipe} \tag{17}$$

$$IC_{y}^{pump} = c^{pump,inst} \cdot \max(0, K_{y}^{pump,new}) \tag{18}$$

$$FOM_{i,y}^{pipe} = c_{i}^{pipe,fom} \cdot \mathbf{A}_{i,y}^{pipe} \tag{19}$$

$$FOM_{y}^{pump} = c^{pump,fom} \cdot K_{y}^{pump} \tag{20}$$

$$VO_{t'}^{pump} = p_{t'}^{e} \cdot w_{t'}^{pump} \tag{21}$$

The heat losses in the heat transmission network do not imply a direct cost for the operator, but the heat losses increase the cost of operation of the system, since the cost of heat applies on the amount of heat that is extracted by the heat extraction system (i.e, q^{ext}), while the heat supplied to the DH network at the outlet of the transmission network is q^{supp} that is computed by taking into account heat losses in the transmission sub-system. Installation costs for the pipes depend on the characteristics of the pipes, among others the insulation layer thickness, inner diameter, and length of the pipes. We calculate coefficients $c_{i}^{pipe,inv}$ (in €) in Equation (22). We adapt the formula provided in (Hirsch et al., 2018) to our case where supply and return pipes are built independently. In this equation L is the distance between the NPP and the DH network (in meter), and D_i is the inner diameter of pipe i (in meter). We assume that supply and return pipes use the same path between the NPP and the DH network.

$$c_{i}^{pipe,inst} = L \cdot (15000 \cdot D_{i}^{2} + 2000 \cdot D_{i} + 500) \tag{22}$$

The minimum and maximum heat load that can transit in the piping system is determined through the regression of the physics-based heat HTN submodel, and given in Equation (23). The numerical values obtained from the regression model for parameters $\underline{\theta}_j$ and $\overline{\theta}$ are provided in the Appendix.

$$\sum_{j \in \mathscr{J}} \underline{\theta}_{j} \cdot \mathbf{U}_{j,t'}^{comb} \leq q_{t'}^{supp} \leq \sum_{j \in \mathscr{J}} \overline{\theta}_{j} \cdot \mathbf{U}_{j,t'}^{comb} \tag{23}$$

Finally, the pumping power is limited by the installed capacity of the pumps (Equation (24)) and depends on the heat load supplied and the combination of pipe used (Equation (25)). The capacity of the pumps at year y, given in Equation (26) depends on the initial pumping capacity and the capacity installed every in between each year block.

$$w_{t'}^{pump} \leq K_{y}^{pump} \tag{24}$$

$$w_{t'}^{pump} = \sum_{j \in \mathscr{J}} f_{j}^{pump}(q_{t'}^{supp}) \cdot \mathbf{U}_{j,t'}^{comb} \tag{25}$$

$$K_{y}^{pump} = \begin{cases} K^{pump,ini} + \sum_{y'=\max(0,y-l_{pump})}^{y} K_{y'}^{pump,new}, & \text{if } y \leq l_{pump} \\ \sum_{y'=\max(0,y-l_{pump})}^{y} K_{y'}^{pump,new}, & \text{otherwise} \end{cases} \tag{26}$$

3.4.5 Alternative heat production capacities

Alternative heat production capacities are modeled as heat sources in which the model can decide to invest at the beginning of any year block. Some of the AHPCs have capacities already installed at the beginning of the simulation horizon, represented with parameters $K_{k}^{capa,ini}$. Moreover, some of the AHPCs may have limitations in the capacity that can be installed due to a limitation in resources (e.g. geothermal plants), or regulatory frameworks (e.g. fossil plants ban). Parameter $\overline{K^{capa}}$ represents the maximum total capacity that can be installed, and $\overline{K^{capa,new}}$ the maximum capacity that can be installed between each year block. The AHPCs have an installation cost (IC^{capa}), a fixed O&M costs (FOM^{capa}), and a variable operation cost (VO^{capa}). These costs and installed capacity constraints of the AHPCs are modeled with the following equations:

$$IC_{k,y}^{capa} = c_{k,y}^{capa,inst} \cdot \max(0, K_{k,y}^{capa,new}) \tag{27}$$

$$FOM_{k,y}^{capa} = c_{k}^{capa,fom} \cdot K_{k,y}^{capa} \tag{28}$$

$$VO_{k,t'}^{capa} = (c_{k}^{capa,vo} + p_{k,t'}^{fuel} / \eta_{k} + p_{t'}^{co2} \cdot EF_{k}^{capa}) \cdot q_{k,t'}^{capa} \tag{29}$$

$$K_{k,y}^{capa} = \begin{cases} K_{k}^{capa,ini} + \sum_{y'=\max(0,y-l_{k})}^{y} K_{k,y'}^{capa,new}, & \text{if } y \leq l_{k} \\ \sum_{y'=\max(0,y-l_{k})}^{y} K_{k,y'}^{capa,new}, & \text{otherwise} \end{cases} \tag{30}$$

$$0 \leq K_{k,y}^{capa} \leq \overline{K_{k}^{capa}} \tag{31}$$

$$K_{k,y}^{capa,new} \leq \overline{K_{k}^{capa,new}} \tag{32}$$

Cost parameter $c_{k,y}^{capa,inst}$, which represents the installation cost per MW of installed capacity, is dependent on the year block y considered. This modeling assumption is made to allow for efficiency progress in manufacturing/installation to be accounted for in the simulation[15]. The capacities are subject to technical constraint regarding maximum heat production and production ramps, modeled in Equations (33) and (34). Parameter $q_{min,k}^{capa}$ corresponds to the minimum heat production of plant k when it is active, and $\mathbf{I}_{k,t'}^{act}$ is a binary variable tracking if AHPC k is active.

$$q_{min,k}^{capa} \mathbf{I}_{k,t'}^{act} \leq q_{k,t'}^{capa} \leq K_{k,y}^{capa} \tag{33}$$

$$-\tau_{k} \cdot \overline{K}_{k}^{capa} \cdot \mathbf{I}_{k,t'}^{act} \leq q_{k,t'}^{capa} - q_{k,t'+1}^{capa} \leq \tau_{k} \cdot \overline{K}_{k}^{capa} \cdot \mathbf{I}_{k,t'}^{act} \tag{34}$$

4 Results and discussion

In this section, we present and discuss the outcomes of the optimization model on the scenarios described in Section 3.2. We compare the following indicators across all scenarios to evaluate the interest of nuclear cogeneration for district heating purposes:

[15] We are not using such feature in the current version of the paper, but future refinement will include these considerations. See for example (Winskel et al., 2024) for literature on heat pump cost reduction as a result of experience gains and learning effects.

- ***Total cost*** of the DH system.
- ***Installed capacities*** of each technology.
- ***Proportion of heat production*** from each technology over the simulation horizon.
- ***Marginal heat cost***, intepreted as a proxy for the heat price on the local heat market.

4.1 Results for the DH system as a whole

4.1.1 System cost comparison

First, we compare the results of the different scenarios from a total cost perspective. Tables 3 and 4 show the total cost of the heat supply system (i.e. the objective function of the optimization problem). We observe that for all local configurations and future scenarios, the availability of nuclear cogeneration as an option to produce heat for the DH system allowed to reduce the total cost, between 2.46% (Geo40-*Ch.Effi* scenario) and 27.9% (Bio20-*Ch.Expan* scenario) for the 0.5TWh case and between 23.1% and 32.3% for the 5TWh case. These results highlight the interest of nuclear cogeneration from the perspective of the local DH system, even in the case of sourcing from nuclear plants located 40 km away. In fact, when the demand is relatively small (0.5TWh case), the cost gains brought by its integration in the optimal mix are lower when the NCP is located 40km away from the DH network than in the 20km cases, but still existant. In the 5TWh case however, these cost gains are almost the same in the 20km and 40km HTN configurations (about 3 points difference). This is mostyl due to the fact that larger amounts of heat transported make high investment costs for pipes more easily recoverable. When the demand is too low, the operation cost gains brought by the NCP integration cannot compensate for the HTN investment costs.

Comparing the 5TWh and 0.5TWh cases other things being equal (intertable comparison), we observe that in all local configurations and prospective scenarios, the total cost gains where higher in relative value in the 5TWh case than in the 0.5TWh case. Moreover, by comparing Geo-type and Bio-type configurations (intercolumn comparison), we observe that the total cost relative gains are slightly higher in Bio-type configurations, but some nuances can be observed. First, compared to low electricity prices, high electricity prices scenarios exhibit higher relative cost gains brought by the integration of the NCP in the Bio-type configurations, while in the Geo-type configurations, high electricity prices scenarios exhibit relative cost gains very close to low electricity prices scenarios (and even a decreasing effect except in 0.5TWh-Geo40 cases). This observation can be explained as follows: in no-nuclear cases, the biomass dominated configurations use much more biomass in the high electricity prices scenarios than in low electricity prices since heat pumps are less cost-competitive (see Figure 10), whereas the geothermal configurations make use of geothermal units with relatively lower variable operation cost. The integration of the NCP therefore replaces a more expensive technology (biomass) in the Bio-type configuration than in the Geo-type configuration (geothermal units). A second observation is that in the 0.5TWh case, decreasing demand scenarios exhibit lower relative cost gains compared to increasing demand scenarios, all other things being equal, in both Geo and Bio-type configurations, with the phenomenon being more pronounced in the Geo-type configurations, whereas the almost no difference is observed in the 5TWh case. This can be explained as follows: in the 5TWh case, the NCP is marginal during less hours compared to the 0.5TWh case (this is true across scenarios and configurations). Therefore, a decrease of the heat demand over years affects mainly the non nuclear technologies in the 5TWh case, while it decreases the nuclear heat production in the 0.5TWh case. This directly translates into an impact on the cost reduction brought by the NCP integration, in relative terms compared to the reference (non nuclear) scenarios. More than the question of the influence of the size of the network on the results, the lesson to be learned from this observation is the following: the integration of a discrete element in the system (pipes the heat transport) generates threshold effects where, for a given scenario, the installation of a pipe is still cost-competitive in a decreasing heat demand perspective, but may or may not bring less cost gains compared to an increasing demand scenario, depending on the marginality of the NCP in this context. This marginality depends on the relative benefits of installing a more or less large pipe.

It is necessary to discuss the decomposition of the system costs in the different scenarios. In fact, the economic interest of nuclear cogeneration cannot be studied solely by quantifying the total system cost. Real-world agents are risk-averse, and the huge up-front investment costs of nuclear cogeneration (both for the heat extraction module and the heat transport network) are costs that cannot be recovered in case of lower than expected demand (e.g. due to more stringent renovation policies). Therefore, economic agents faced with the choice of investing either in a highly capitalistic technology or in a more expensive but less capitalistic technology may not make the same choices as a central planner with perfect foresight and rational expectations.

4.1.2 Optimal mixes

A-type scenarios Figure 6 shows the resulting heat production capacities available at each simulated year for configurations **Geo∅**, Geo20 and Geo40 in the 0.5TWh. We observe that in all scenarios the investment in pipes for nuclear heat transmission is realized as soon as the NCP is available (in 2035)[16], except in the decreasing demand and low electricity prices scenario in the 40km HTN configuration, where it is postponed until 2050. In the latter case, this delay is justified by the insufficient heat demand, which does not support the decommissioning of geothermal and gas units before their expiration. Electricity prices being low, the difference in operating cost between nuclear energy and geothermal pumps is not sufficient to offset the high infrastructure cost required for the HTN, making it economically viable to continue using geothermal units until their expiration. Moreover, one can note that in this context, heat pump (HP) units are only used as a transitional measure, whereas in all other cases where NCP is available, non geothermal heat pumps are only installed in 2055.

Conversely, in the *Favored Expansion* scenario in the 20km configuration, the increased heat demand justifies the early adoption of nuclear cogeneration technology, and the anticipated decomissioning of biomass and gas units, as well as most geothermal capacities. In this scenario, no heat pump or geothermal unit is installed after 2050, and the NCP provides all the required heat (with the SWI in base load) starting 2055. This is achieved by the installation of a second smaller pipe to fullfill the demand in the summer season when the demand is very low (around 15MW)[17].

[16] Note that in our setting, the heat extraction capacity on the NCP is installed in 2035. We assumed no possible retrofit, so the extraction capacity is installed once for all, even if transmission pipes are only installed 15 years later.

[17] Pipes have a technical minimum in term of acceptable water velocity, that translates in a lower bound of tranportable heat. Therefore, large pipes cannot sustain a very low summer heat supply rate.

Table 3: Total discounted cost (B€) and relative deviation from baseline without nuclear, for the 0.5TWh cases

Prospective scenarios			Local configurations					
Scenario	Heat demand	Electricity price	**GeoØ**	Geo20	Geo40	**BioØ**	Bio20	Bio40
Favored Expansion	↗	Low	0.704	0.538 **(-23.5%)**	0.625 **(-11.3%)**	0.832	0.632 **(-24.0%)**	0.718 **(-13.7%)**
Chosen Expansion	↗	High	1.12	0.864 **(-23.1%)**	0.971 **(-13.6%)**	1.27	0.921 **(-27.9%)**	1.03 **(-19.4%)**
Chosen Efficiency	↘	Low	0.519	0.436 **(-15.9%)**	0.506 **(-2.46%)**	0.643	0.521 **(-18.9%)**	0.594 **(-7.67%)**
Constrained Efficiency	↘	High	0.839	0.724 **(-13.7%)**	0.817 **(-2.71%)**	0.982	0.748 **(-23.8%)**	0.872 **(-11.2%)**

Local configurations naming: Geo and Bio refer to the initial heat production mix, Ø, 20 and 40 refer to nuclear plant being respectively "not available", "available and located at 20km", "available and located at 40km".
Prospective scenarios: Each row correspond to a prospective scenario.
Relative deviation: The bold numbers in brackets indicate the relative *Relative deviation*: The bold numbers in brackets indicate the relative deviation between the local configuration (Geo20, Geo40, etc.) and the reference case (**GeoØ** or **BioØ**).

Table 4: Total discounted cost (B€) and relative deviation from baseline without nuclear, for the 5TWh cases

Prospective scenarios			Local configurations*					
Scenario	Heat demand	Electricity price	**GeoØ**	Geo20	Geo40	**BioØ**	Bio20	Bio40
Favored Expansion	↗	Low	7.08	5.07 **(-28.4%)**	5.28 **(-25.4%)**	8.36	5.97 **(-28.5%)**	6.19 **(-26.0%)**
Chosen Expansion	↗	High	11.2	8.19 **(-27.1%)**	8.50 **(-24.3%)**	12.7	8.71 **(-31.8%)**	9.02 **(-29.4%)**
Chosen Efficiency	↘	Low	5.23	3.81 **(-27.1%)**	4.00 **(-23.5%)**	6.47	4.67 **(-27.8%)**	4.86 **(-24.8%)**
Constrained Efficiency	↘	High	8.39	6.19 **(-26.2%)**	6.45 **(-23.1%)**	9.82	6.64 **(-32.3%)**	6.91 **(-29.6%)**

Local configurations naming: Geo and Bio refer to the initial heat production mix, Ø, 20 and 40 refer to nuclear plant being respectively "not available", "available and located at 20km", "available and located at 40km".
Prospective scenarios: Each row correspond to a prospective scenario.
Relative deviation: The bold numbers in brackets indicate the relative deviation between the local configuration (Geo20, Geo40, etc.) and the reference case (**GeoØ** or **BioØ**).

Figure 6: Installed capacities (MW) for the 0.5TWh case in Geo-type configurations.

Figure 7: Heat production (GWh) over the optimization horizon for the 0.5TWh case in Geo-type configurations.

In addition, we observe that the electricity price has some impact on the results. In fact, the main difference is twofold: First, in the ten first years, geothermal units are less used and biomass and gas units more used in high electricity price scenarios, compared to low

electricity price scenarios. Second, in the last ten years of the horizon, in scenarios where the electricity price is low, heat pumps are favored to replace expiring geothermal units due to their relatively smaller installation cost. The minimal impact for the rest of the results can be attributed to a combination of different factors. The need for decarbonization renders the use of gas units non-viable, and the high cost of biomass makes it a non-competitive low carbon option. Consequently, the remaining units all have variable costs proportional to the electricity price (as a fuel for HP and geothermal, and as a multiplier of the opportunity cost and pumping cost for nuclear cogeneration). Therefore, the electricity price levels only adjust all variable costs up and down, making the trade-off decision between heat pumps, geothermal energy, and nuclear cogeneration primarily an arbitrage between variable operation costs and capital costs. In our setting, it is clear that this has very little influence on the final result. One should note that this outcome is influenced by modeling choices. In practice, contracts between nuclear cogeneration units and district heating (DH) operators might differ from pure hourly opportunity cost pricing, potentially altering the balance between nuclear cogeneration and heat pumps. Nuclear cogeneration could offer more stable heat costs, which is not represented in this model.

Finally, an interesting observation concerns the size of pipes installed. In the *Chosen Efficiency* scenarios (in both 20 and 40km configurations), the smallest pipe (DN300) is installed, while the second pipe (DN500) is installed in all other cases. Interestingly, the NCP extraction capacity is higher in the *Ch.Effi* than in the *Con.Effi* scenarios, which seems counter-intuitive since a smaller pipe means higher specific pumping costs. In the 40km configuration, this could be explained by the late investment in the piping system. However, in the 20km configuration, this can only be attributed to the relatively low electricity prices, which imply relatively low pumping costs, and hence justify the use of a smaller pipe for which investment costs are reduced.

Figures 8 and 9 show the results of the optimization for the 5TWh case in Geo-type local configurations, in terms of installed heat production capacities and total heat production by each technology. This time, all scenarios exhibit early investment in HTN infrastructures. This can be interpeted as the heat demand being high enough to justify the investment with huge capex, and decomissionning of the gas plants before their expiration, even in the *Chosen Efficiency*-40km case. We also note the same differences between the high and low electricity price scenarios as in the 0.5TWh case. Common to every scenario is the fact that heat pumps are used to fullfill the peak heat demand after 2050. In fact, heat pumps cover a greater share of the heat supply in the increasing demand prospective scenarios (*Fav.Expan* and *Ch.Expan*) in the 5TWh case than in the 0.5TWh case. Since this supplemental share of heat produced by heat pumps is located in peak hours, the difference between the 0.5TWh and 5TWh cases is most visible in the installed capacities (Figures 6 and 8). On the contrary, in the decreasing demand scenarios, heat pumps share of heat supply is disminished, due to the coupled effect of large HTN pipes investment costs being more easily recovered, and having less hours in the summer where the HTN must be turned off for technical minimum requirements compared to the 0.5TWh cases. The latter reason also explains why in the decreasing demand scenarios, the geothermal-to-NCP ratio remains unchanged in terms of installed capacities in the 5TWh compared to 0.5TWh case, while geothermal units almost disappear from the heat supply graphs in the 5TWh case (Figure 9). Indeed, geothermal units are stil lneeded for the peak hours, but not necessary anymore in the low demand summer hours.

Finally, in all scenarios in the 5TWh case, the large pipe is installed and used at saturation (the heat extraction capacity installed on the NCP equals the maximum transportable heat of the pipe), while in the 0.5TWh case, the HTN pipes where only saturated when the smallest pipe was installed (which happens in *Ch.Effi* scenarios outcomes). We observe that this saturation is also happening in the 40km HTN configuration, and therefore that the NCP-to-DH distance has no impact on the optimal mix trajectory.

Figure 8: Installed capacities (MW) for the 5TWh case in Geo-type configurations.

B-type scenarios Figures 10 and 11 show the installed heat production capacities and the total heat production of each technology for the 0.5TWh cases in Bio-type local configurations. In terms of NCP use, the result is very similar to the 0.5TWh Geo-type cases, with the NCP becoming the main source of heat after 2035, gas burners being decomissioned before their expiration, and some low carbon conventional capacity being maintained to fulfill the low summer demand (below technical minimum of the HTN) and the winter peak demand.

Contrary to the Geo-type configurations results, even in the 40km *Chosen Efficiency* scenario, the HTN is installed as early as 2035. This is due to biomass being less cost-competitive than geothermal pumps, making the NCP+HTN a cost-competitive option to replace most biomass capacity as early as 2035 even in the less favorable scenario.

Moreover, the complementarity between biomass and NCP in the Bio-type configurations is different from the one between geothermal pumps and NCP in the Geo-type configurations. In the low electricity price scenarios, the Bio-configurations optimal trajectories install heat pumps to replace biomass and gas capacities, while in the Geo-type configurations, additional geothermal heat pumps are installed but replace less gas burners. In the high electricity scenarios, heat pumps are installed in the Bio-type configurations to re-

Figure 9: Heat production (GWh) over the optimization horizon for the 5TWh case in Geo-type configurations.

Figure 10: Installed capacities (MW) for the 0.5TWh case in Bio-type configurations.

Figure 11: Heat production (GWh) over the optimization horizon for the 0.5TWh case in Bio-type configurations.

place biomass starting 2030, while in the Geo-type configurations, additional geothermal units are built and no heat pump is installed before 2055 (except in the 40km-*Con.Effi* scenario). These observations are mainly due to the biomass variable operation costs being relatively higher than those of geothermal pumps. In addition, contrary to the Geo-type configurations where heat pumps where present after 2050 in all 20km scenarios, only biomass and SWI complements the NCP heat supply in the Bio-type configurations.

Another distinction in the results of optimal production mix between Geo-type and Bio-type configurations lies the pipes installed. In the latter configurations, the smallest pipe is also the one installed in 2035 in the 40km-*Ch.Effi* and 20km-*Con.Effi* scenarios as the only pipe, and in 2050 in the 20km-*Ch.Expan* scenario (to complement the DN500 pipe in the low demand summer weeks). The small pipe installation in 2050 is favored by the expiration in biomass units in 2050 (whereas geothermal units expired in 2055 in the Geo-type configurations). For the cases where 2035 installation, the Bio40-*Ch.Effi* scenario is more favorable to nuclear cogeneration than the Geo40-*Ch.Effi*, due to the absence of geothermal pumps, which explains the earlier investment in the HTN.

Figures 12 and 13 show the results of the optimization for the 5TWh case in Bio-type local configurations. Similar to the Geo-type configurations, we can observe that in all scenarios the HTN infrastructure is installed as soon as 2035 to replace the gas capacities and part of the biomass capacities. Again, this is the case even in the 40 km HTN configurations. In addition, as in the Geo-type configurations, the heat demand is large enough in the 5TWh case so that non-nuclear capacities are only installed for peak demand but not for the low demand summer season (i.e, the technical minimum of pipes is not an issue here). Finally, similar to the Geo-type configurations, the largest pipe is used at saturation, and the NCP-to-DH distance has no impact on the optimal mix trajectory.

First, compared to the 0.5TWh case, in the high electricity scenarios, biomass represent a higher share of the heat supplied. In the low electricity scenarios, the role of biomass is more nuanced. It plays a bigger (resp. smaller) role in the increasing (resp. decreasing) demand scenarios compared to 0.5TWh cases.

In addition, the differences between Bio and Geo-type configurations noted for the 0.5TWh case in terms of complementarity of

the technologies still apply in the 5TWh case.

Figure 12: Installed capacities (MW) for the 5TWh case in Bio-type configurations.

Figure 13: Heat production (GWh) over the optimization horizon for the 5TWh case in Bio-type configurations.

4.1.3 Marginal cost of heat

We use the marginal cost of heat as proxy to analyze what would be the change in heat pricing for the final consumer in district heating adopting nuclear cogeneration, if the pricing was based on marginal cost tarification. Figures 14 and 15 show the marginal heat cost duration curves for the 0.5TWh and 5TWh cases.

Left parts of the marginal cost duration curves in a stairs shape correspond to periods where gas burners are the marginal technology. Even though gas is substituted more quickly in the Geo20 and Bio20 configurations compared to others, it is still the marginal technology during a significant part of the winter season in the first years of the simulation horizon, and particularly during peak hours. Therefore, the marginal heat cost curves shift to the left, but keep the stair shape for the most left par tof it. In Bio-type configurations, the staircase parts correspond both to gas burners and biomass marginal hours (gas being at the very left, and biomass being in between the staircase portion and the continuous slope portion). The duration during which biomass is marginal decreases when NCP is introduced, shifting the curve to the left. This is especially true in the 20 km cases, but can also be slightly noticed in the 40 km cases.

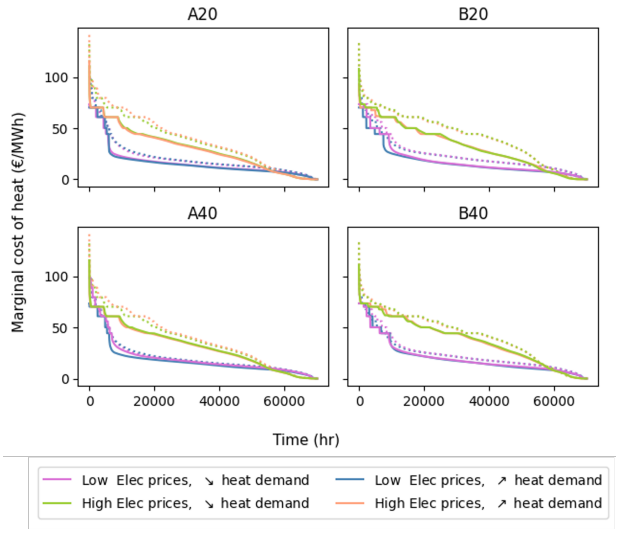

Figure 14: Marginal heat cost duration curves for the 0.5TWh cases.
Legend: Solid lines correspond to scenarios with NCP. Dotted lines correspond to no NCP (**GeoØ** and **BioØ**) scenarios.
NB: Orange and green dotted curves overlap in the Geo20 and Geo40 cases.

We also observe that the marginal cost reduction is more important in the 5TWh case than in the 0.5TWh case, especially for high electricity prices scenarios. This is also particularly true for the 40 km configurations, and correlates with the higher system cost gains obtained in the 5TWh-40km configurations compared to the 0.5TWh-40km configurations. In general, the NCP is marginal after 2035 for a significant part of the hours in all scenarios except the low electricity decreasing demand Geo40 configuration, driving the marginal cost down in comparison with the reference no-nuclear case where heat pumps (which have a higher variable operation cost) are the main marginal technology. For the exception mentioned, we observe that marginal cost gains are very small, which is mainly explained by the delayed investment in the HTN in 2050 instead of 2035.

In addition, one can note the elbow shape of the blue and pink curves (i.e low electricity prices), exhibiting a rapid drop of marginal

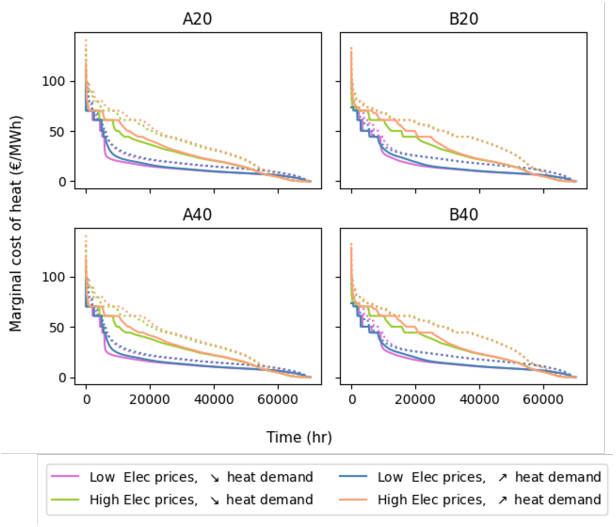

Figure 15: Marginal heat cost duration curves for the 5TWh cases.
Legend: Solid lines correspond to scenarios with NCP. Dotted lines correspond to no NCP (**Geo∅** and **Bio∅**) scenarios.
NB: Orange and green dotted curves overlap in the Geo20 and Geo40 cases.

costs. It is mainly due to the dual effect of the inclusion of nuclear cogeneration after 2035 which drives the marginal cost down, and of marginal costs being already relatively low in most hours due to geothermal units being marginal in a context of low electricity prices. In the small DH (0.5TWh) case, this drop is more pronounced in the increasing demand scenario, whereas it is more noticeable in the increasing demand scenario in the case of relatively large DH networks (5TWh).

Finally, it should be noted that one significant effect of the NCP integration in the heat mix does not appear on this representation of marginal costs duration curve for the full horizon. In the first ten years of the horizon, the optimal mixes have higher marginal costs in the cases with nuclear (Geo20, Geo40, Bio20, and Bio40) than in the cases without (**Geo∅** and **Bio∅**). Indeed, there is a threshold effect due to the availability of the NCP after 2035. The optimal mix results in the scenarios with nuclear power show that it is economically more attractive to invest in the NCP-HTN than not to, even if it is not available until 2035. But in this case, it is not worth investing massively in the first ten years in geothermal or heat pump capacity, which will be under-utilized once the NCP is available. Therefore, the marginal cost gains obtained with the NCP integration in the mix are not homogeneously distributed in time.

4.1.4 GHG emissions

Figures 16 and 17 show the GHG intensity of heat evolution for all scenario considered.

First, we observe that the decarbonization trajectory is faster than the set emissions cap in most scenarios, showing that the "national carbon price" set as well as the fuel cost make gas burners too costly and discard them naturally from the optimal mix, even without an emission cap. There could be an interest to try with a tighter emission cap and see how gas burners are replaced. Moreover, there is an acceleration of the GHG intensity drop in 2035 for scenarios where the NCP is available, which is not observed in non nuclear scenarios. This discrepancy can be explained by the binary nature of the nuclear cogeneration infrastructure, in contrast to other heat sources. Heat pumps, biomass, SWI and geothermal capacities are continuous variables that can be adjusted to meet decarbonization targets at the lowest possible cost. However, nuclear heat must pass through the HTN piping system, which is inherently binary in its investment decisions. Pipes available for installation have defined discrete sizes, resulting in threshold effects. As observed for instance on Figure 17 in the 0.5TWh-Bio20-*Ch.Expan* case, the least-cost optimal decarbonization path involves early investment in HTN infrastructure and an early phase-out of gas combustion. In fact, the high investment cost of the HTN justifies its use at relatively high capacity factors, i.e. it almost completely satisfies the heat demand and thus reduces the production of other technologies. Similarly, the use of gas burners in the 5TWh-Geo20-*Fav.Expan* scenario drops to almost zero once the NCP becomes available.

As observed on Figures 16 and 17, scenarios with low electricity prices scenarios (*Fav.Expan* and *Ch.Effi*) exhibit a lower initial GHG intensity than the high electricity prices scenarios (*Ch.Expan* and *Con.Effi*). In fact we have given the model the option to invest in new capacities as early as 2025, which, in the case of the low electricity prices scenarios in the Geo-type configurations (Figure 16), lead the investment in additional geothermal capacities in 2025 for low cost base heat production. Given that geothermal is much less GHG-intensive than gas, this early investment translates into a significantly lower GHG initial intensity. In the case of Bio-type configurations (Figure 17), heat pumps are installed in 2025 to complement biomass and some gas capacities.

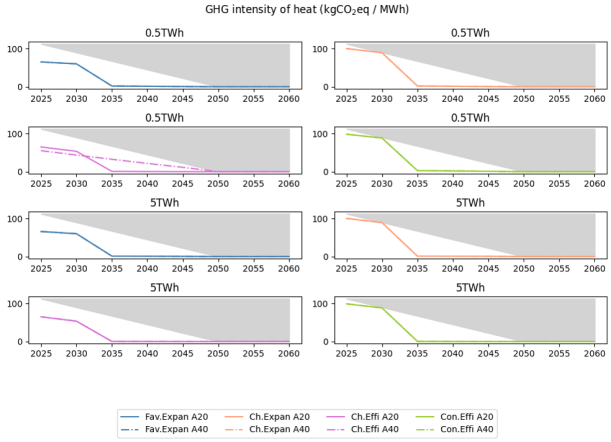

Figure 16: GHG intensity of heat for Geo-type configurations.

5 Conclusion

The path to fully decarbonizing heat production for district heating networks involves huge investments in low-carbon technologies. In all local configurations and prospective scenarios studied, massive investment in low-carbon heat sources is realized to substitute aging capacities and phase-out of natural gas in heat production. The results obtained from our modeling approach indicate that, under our assumptions on technology availability, energy and installation costs, the least-cost decarbonization pathways make use of nuclear cogeneration at some point to supply a significant part of the heat demand. The investment in heat extraction capacities to make the nuclear plant a cogeneration plant and in the heat transmission network to replace gas burners as well as aging low carbon capacities is realized in all scenarios considered. Four main conclusions can be drawn from our results.

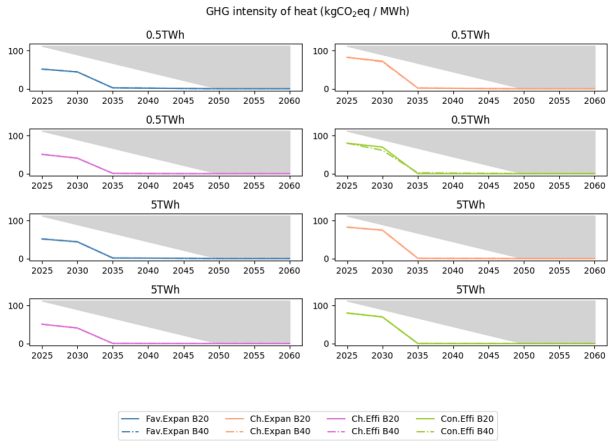

Figure 17: GHG intensity of heat for Bio-type configurations.

First, the total discounted system cost gains obtained by including the option to invest in nuclear cogeneration ranges from 2.5% in our least favorable scenario (corresponding to a 0.5TWh/a DH demand in a geothermal-dominated initial mix, a 40km nuclear heat transport distance, and a decreasing heat demand combined to rather low electricity prices) to 32.3% (in a 5TWh/a case with a biomass-dominated initial heat production mix, a 20km nuclear heat transport distance, and a decreasing heat demand with rather high electricity prices). In addition, the initial heat production have some impact on the system cost relative gains brought by nuclear cogeneration integration, with biomass-initially dominated benefiting more it than geothermal-initially dominated production mix. The distance of nuclear heat transport does have an impact on the system cost relative gains achievable, but this impact is largely attenuated in the case of a 5TWh/a district heat compared to the 0.5TWh/a case.

Second, most scenarios exhibit an early investment in nuclear heat transmission infrastructures, while our least favorable scenario (a decreasing demand combined with low electricity in a rather small district heating network located 40km away from the nuclear plant) only exhibits investment in these infrastructures in 2050. In all scenarios but the latter, the investment in nuclear heat tranmission infrastructures is beneficial overall to the system, and the high installation cost justifies an early investment to benefit for long enough of the operation cost savings. In the case of an installation in 2050, the heat load quantities and the economic factors incentivize to use existing capacities for a relatively longer time, and to install heat pump and geothermal capacities to compensate for natural gas phase out.

As far as GHG emissions are concerned, the early investment and the binary nature of investment in heat transmission infrastructures creates a threshold effect in 2035 which accelerates the drop of GHG emissions. In most scenarios, results exhibit the economic benefits to decarbonize more rapidly than the emission cap we set, due to increasing gas prices as well as the national CO_2 price enforced.

Finally, the results on system cost relative gains, installed capacities and dispatch among heat sources vary little accross electricity prices prospective scenarios, other things being equal. The fact that both the opportunity cost of nuclear heat, and the variable operation cost of heat pumps and geothermal units scale with electricity prices explains much of this result. We would certainly obtain different results if we were to model differently the way the NCP is bidding into the local heat market.

The latter observation is one of the limits of the model developed and used in this paper. Future research could explore different pricing mechanisms for the nuclear cogenerated heat, not directly correlated to the price of electricity. Other limits can be mentioned and would require further work to overcome.

For instance, because we assume perfect foresight and rational expectation from the central planner, we did not consider any need for backup capacities to prevent for the risk of lost load in the case of unexpected shutdown of the heat production units. The fact that the nuclear cogeneration plant provides as much as 90% of the annual heat demand after 2035 in most of our in our scenarios exacerbate this question. Results on system costs gains comparison would be affected if the need for back-up units were to be considered.

In addition, sensitivities to other parameters (discount rate, specific investment costs, efficiency, stringency of emissions caps) can be tested and compared with the variations in our key indicator values across the scenarios considered.

Finally, to demonstrate the interest of the multi-period approach developed in the paper in identifying non linear effects and variations in technology development trajectories between the scenarios, a quantivative comparison between a static one-year mix optimization and our multi-period optimization should be carried out. We could compare the results on our key indicators obtained with the former with those shown in the paper.

These are all elements that can be studied in future research.

References

A. Gabbar, H., Abdussami, M. R., & Adham, M. I. (2020). Techno-economic evaluation of interconnected nuclear-renewable micro hybrid energy systems with combined heat and power [Number: 7 Publisher: Multidisciplinary Digital Publishing Institute]. *Energies*, *13*(7), 1642. https://doi.org/10.3390/en13071642

Abushamah, H. A. S., Burian, O., & Škoda, R. (2023). Design and operation optimization of a nuclear heat-driven district cooling system [Publisher: Hindawi]. *International Journal of Energy Research*, *2023*, e7880842. https://doi.org/10.1155/2023/7880842

Buonomo, B., Ciccarelli, V., Manca, O., Nardini, S., & Plomitallo, R. (2022). Effect of nanofluid on a low-enthalpy geothermal plant. *Journal of Physics: Conference Series*, *2385*, 012018. https://doi.org/10.1088/1742-6596/2385/1/012018

Carlsson, J., Shropshire, D. E., van Heek, A., & Fütterer, M. A. (2012). Economic viability of small nuclear reactors in future european cogeneration markets. *Energy Policy*, *43*, 396–406. https://doi.org/10.1016/j.enpol.2012.01.020

Chau, J., Sowlati, T., Sokhansanj, S., Preto, F., Melin, S., & Bi, X. (2009). Techno-economic analysis of wood biomass boilers for the greenhouse industry [Number: 3]. *Applied Energy*, *86*(3), 364–371. https://doi.org/10.1016/j.apenergy.2008.05.010

Chen, J., Zheng, W., Kong, Y., Yang, X., Liu, Z., & Xia, J. (2021). Case study on combined heat and water system for nuclear district heating in jiaodong peninsula. *Energy*, *218*, 1–10. https://doi.org/10.1016/j.energy.2020.119546

Dong, Z., Li, B., Li, J., Guo, Z., Huang, X., Zhang, Y., & Zhang, Z. (2021). Flexible control of nuclear cogeneration plants for balancing intermittent renewables. *Energy*, *221*, 12. https://doi.org/10.1016/j.energy.2021.119906

Edwards, J., Bindra, H., & Sabharwall, P. (2016). Exergy analysis of thermal energy storage options with nuclear power plants. *Annals of Nuclear Energy*, *96*, 104–111. https://doi.org/10.1016/j.anucene.2016.06.005

El Mrabet, S., Lamrani, B., Abd-Lefdil, M., & Kousksou, T. (2024). A brief overview of district heating pipe network progress. *Energy Conversion and Management: X*, *23*, 100641. https://doi.org/10.1016/j.ecmx.2024.100641

Enerdata. (2023, November 24). *Carbon price forecast 2030-2050: Assessing market stability & future challenges*. Retrieved August 22, 2024, from https://www.enerdata.net/publications/executive-briefing/carbon-price-projections-eu-ets.html

Energy Information Administration - EIA. (2021, October 6). *International energy outlook 2021*. Retrieved August 23, 2024, from https://www.eia.gov/outlooks/ieo/consumption/sub-topic-03.php

ETI. (2016, September). *System requirements for alternative nuclear technologies* (Archive Location: https://www.eti.co.uk/ Publisher: The ETI). Retrieved April 22, 2024, from https://www.eti.co.uk/library/system-requirements-for-alternative-nuclear-technologies-phase-3

European Commission. (2014). *Guide to cost-benefit analysis of investment projects: Economic appraisal tool for cohesion policy 2014-2020*. https://ec.europa.eu/regional_policy/en/information/publications/guides/2014/guide-to-cost-benefit-analysis-of-investment-projects-for-cohesion-policy-2014-2020

Eurostat. (2022). *Disaggregated final energy consumption in households*. Retrieved August 21, 2024, from https://ec.europa.eu/eurostat/databrowser/view/nrg_d_hhq/default/table?lang=en

Fehrenbach, D., Merkel, E., McKenna, R., Karl, U., & Fichtner, W. (2014). On the economic potential for electric load management in the german residential heating sector – an optimising energy system model approach. *Energy*, *71*, 263–276. https://doi.org/10.1016/j.energy.2014.04.061

Fridleifsson, I. B. (2001). Geothermal energy for the benefit of the people [Number: 3]. *Renewable and Sustainable Energy Reviews*, *5*(3), 299–312. https://doi.org/10.1016/S1364-0321(01)00002-8

Hadi Ghazaie, S., Sadeghi, K., Chebac, R., Sokolova, E., Fedorovich, E., Cammi, A., Enrico Ricotti, M., & Saeed Shirani, A. (2022). On the use of advanced nuclear cogeneration plant integrated into latent heat storage for district heating. *Sustainable Energy Technologies and Assessments*, *50*, 14. https://doi.org/10.1016/j.seta.2021.101838

Hast, A., Syri, S., Lekavičius, V., & Galinis, A. (2018). District heating in cities as a part of low-carbon energy system. *Energy*, *152*, 627–639. https://doi.org/10.1016/j.energy.2018.03.156

Helistö, N., Kiviluoma, J., Holttinen, H., Lara, J. D., & Hodge, B.-M. (2019). Including operational aspects in the planning of power systems with large amounts of variable generation: A review of modeling approaches [_eprint: https://onlinelibrary.wiley.com/doi/pdf/10.1002/wene.341]. *WIREs Energy and Environment*, *8*(5), e341. https://doi.org/10.1002/wene.341

Helistö, N., Kiviluoma, J., Ikäheimo, J., Rasku, T., Rinne, E., O'Dwyer, C., Li, R., & Flynn, D. (2019). Backbone—an adaptable energy systems modelling framework [Number: 17 Publisher: Multidisciplinary Digital Publishing Institute]. *Energies*, *12*(17), 3388. https://doi.org/10.3390/en12173388

Helistö, N., Kiviluoma, J., & Reittu, H. (2020). Selection of representative slices for generation expansion planning using regular decomposition. *Energy*, *211*, 118585. https://doi.org/10.1016/j.energy.2020.118585

Hirsch, P., Duzinkiewicz, K., Grochowski, M., & Piotrowski, R. (2016). Two-phase optimizing approach to design assessments of long distance heat transportation for CHP systems. *Applied Energy*, *182*, 164–176. https://doi.org/10.1016/j.apenergy.2016.08.107

Hirsch, P., Grochowski, M., & Duzinkiewicz, K. (2018). Decision support system for design of long distance heat transportation system. *Energy and Buildings*, *173*, 378–388. https://doi.org/10.1016/j.enbuild.2018.05.010

Hotmaps Project. (2021, January). *Hotmaps - heating & cooling outlook until 2050, EU-28*.

IAEA. (2019). *Guidance on nuclear energy cogeneration*.

IAEA. (2000). *Introduction of nuclear desalination: A guidebook*. International Atomic Energy Agency.

IAEA. (2020). *Nuclear power reactors in the world* (Text) (ISBN: 9789201148209 Publication Title: Nuclear Power Reactors in the World). International Atomic Energy Agency. Retrieved August 20, 2024, from https://www.iaea.org/publications/14756/nuclear-power-reactors-in-the-world

IAEA. (2017). *Opportunities for cogeneration with nuclear energy*.

IEA. (2023a). *CO2 emissions in 2023*.

IEA. (2023b). *Net zero roadmap: A global pathway to keep the 1.5 °c goal in reach - 2023 update*.

IEA. (2023c). *Renewables 2023*. Retrieved August 23, 2024, from https://www.iea.org/reports/renewables-2023

IEA. (2023d). *World energy outlook 2023*.

IPCC. (2022). *Working group III contribution to the sixth assessment report of the intergovernmental panel on climate change*.

Lavialle, G., Crevon, S., Ruby, A., Cardoso, G., Goicea, A., Vobr, F., Zezula, L., Ikonen, J.-P., & Soppela, O. (2023, September). *D3.1 definition of case studies for techo-economic analyses including some environmental aspects* (No. D3.1). Retrieved December 1, 2023, from http://tandemproject.eu/wp-content/uploads/2023/09/D3_1_Definition_of_case_studies_for_techno_economic_analyses_including_some_environmental_aspects_V1.pdf

Leurent, M., Da Costa, P., Jasserand, F., Rämä, M., & Persson, U. (2018). Cost and climate savings through nuclear district heating in a french urban area. *Energy Policy*, *115*. https://doi.org/10.1016/j.enpol.2018.01.043

Leurent, M., Da Costa, P., Rämä, M., Persson, U., & Jasserand, F. (2018). Cost-benefit analysis of district heating systems using heat from nuclear plants in seven european countries. *Energy*, *149*, 454–472. https://doi.org/10.1016/j.energy.2018.01.149

Leurent, M., Jasserand, F., Locatelli, G., Palm, J., Rämä, M., & Trianni, A. (2017). Driving forces and obstacles to nuclear cogeneration in europe: Lessons learnt from finland. *Energy Policy*, *107*. https://doi.org/10.1016/j.enpol.2017.04.025

Li, Y., Pan, W., Xia, J., & Jiang, Y. (2019). Combined heat and water system for long-distance heat transportation. *Energy*, *172*, 401–408. https://doi.org/10.1016/j.energy.2019.01.139

Lindroos, T. J., Pursiheimo, E., Sahlberg, V., & Tulkki, V. (2019). A techno-economic assessment of NuScale and DHR-400 reactors in a district heating and cooling grid. *Energy Sources, Part B: Economics, Planning, and Policy*, *14*(1), 13–24. https://doi.org/10.1080/15567249.2019.1595223

Lipka, M., & Rajewski, A. (2020). Regress in nuclear district heating. the need for rethinking cogeneration. *Progress in Nuclear Energy*, *130*, 103518. https://doi.org/10.1016/j.pnucene.2020.103518

Liu, W., Sun, Z., Liu, X., Li, G., Wang, J., & Yan, J. (2023). Capacity and operation optimization of a low-temperature nuclear heating system considering heat storage. *Progress in Nuclear Energy*, *161*, 104717. https://doi.org/10.1016/j.pnucene.2023.104717

Locatelli, G., Fiordaliso, A., Boarin, S., & Ricotti, M. E. (2017). Cogeneration: An option to facilitate load following in small modular reactors. *Progress in Nuclear Energy*, *97*, 153–161. https://doi.org/10.1016/j.pnucene.2016.12.012

Meesenburg, W., Ommen, T., & Elmegaard, B. (2018). Dynamic exergoeconomic analysis of a heat pump system used for ancillary services in an integrated energy system. *Energy*, *152*, 154–165. https://doi.org/10.1016/j.energy.2018.03.093

NEA & OECD. (2022, July). *Beyond electricity*. OECD. https://doi.org/10.1787/bed3e52c-en

Odyssee-Mure. (2020). *International comparisons of household energy efficiency*. Retrieved August 20, 2024, from https://assets.publishing.service.gov.uk/media/5e7b58fcd3bf7f133f849328/International_comparisons_of_household_energy_efficiency_2020.pdf

Pavičević, M., Novosel, T., Pukšec, T., & Duić, N. (2017). Hourly optimization and sizing of district heating systems considering building refurbishment – case study for the city of zagreb. *Energy*, *137*, 1264–1276. https://doi.org/10.1016/j.energy.2017.06.105

Pursiheimo, E., Lindroos, T. J., Sundell, D., Rämä, M., & Tulkki, V. (2022). Optimal investment analysis for heat pumps and nuclear heat in decarbonised helsinki metropolitan district heating system. *Energy Storage and Saving*, *1*(2), 80–92. https://doi.org/10.1016/j.enss.2022.03.001

Quinet, A., Bueb, J., Hir, B. L., Mesqui, B., Pommeret, A., & Combaud, M. (2019, February). *La valeur de l'action pour le climat*.

Rämä, M., Leurent, M., & Devezeaux de Lavergne, J. G. (2020). Flexible nuclear co-generation plant combined with district heating and a large-scale heat storage. *Energy*, *193*. https://doi.org/10.1016/j.energy.2019.116728

RTE. (2023). *Futurs énergétiques 2050*. https://www.rte-france.com/analyses-tendances-et-prospectives/bilan-previsionnel-2050-futurs-energetiques#Lesdocuments

RTE & ADEME. (2021). *Réduction des émissions de CO2, impact sur le système électrique : Quelle contribution du chauffage dans les bâtiments à l'horizon 2035 ?* Retrieved August 21, 2024, from https://assets.rte-france.com/prod/public/2020-12/Rapport%20chauffage_RTE_Ademe.pdf

Ruhnau, O., Hirth, L., & Praktiknjo, A. (2019). Time series of heat demand and heat pump efficiency for energy system modeling [Publisher: Nature Publishing Group]. *Scientific Data*, *6*(1), 189. https://doi.org/10.1038/s41597-019-0199-y

Safa, H. (2012). Heat recovery from nuclear power plants. *International Journal of Electrical Power & Energy Systems*, *42*(1), 553–559. https://doi.org/10.1016/j.ijepes.2012.04.052

van der Heijde, B., Scapino, L., Vandermeulen, A., Patteeuw, D., Salenbien, R., & Helsen, L. (2018). Using representative time slices for optimization of thermal energy storage systems in low-temperature district heating systems: 31st international conference on efficiency, cost, optimization, simulation and environmental impact of energy systems, (ECOS 2018) [Place: Guimarães Publisher: University of Minho Press]. *ECOS 2018 - Proceedings of the 31st International Conference on Efficiency, Cost, Optimization, Simulation and Environmental Impact of Energy Systems*. Retrieved August 21, 2024, from http://www.scopus.com/inward/record.url?scp=85064172415&partnerID=8YFLogxK

Vandermeulen, A., van der Heijde, B., & Helsen, L. (2018). Controlling district heating and cooling networks to unlock flexibility: A review. *Energy*, *151*, 103–115. https://doi.org/10.1016/j.energy.2018.03.034

Värri, K., & Syri, S. (2019). The possible role of modular nuclear reactors in district heating: Case helsinki region [Number: 11 Publisher: Multidisciplinary Digital Publishing Institute]. *Energies*, *12*(11), 2195. https://doi.org/10.3390/en12112195

Winskel, M., Heptonstall, P., & Gross, R. (2024). Reducing heat pump installed costs: Reviewing historic trends and assessing future prospects. *Applied Energy*, *375*, 124014. https://doi.org/10.1016/j.apenergy.2024.124014

Xu, C., Khan, M. S., Kong, F., Yu, D., Yu, J., & Li, T. (2021). Conceptual design and optimization of cogeneration system based on small modular lead-cooled fast reactor. *Energy Science & Engineering*, *9*(10), 1688–1702. https://doi.org/10.1002/ese3.942

6 Appendix

6.1 Nomenclature

Acronym	Description	Remark
DH	District Heating	Section 3.1 for more details
NCP	Nuclear Cogeneration Plant	
AHCP	Alternative Heat Production Capacity	
HTN	Heat Transmission Network	
0.5TWh , 5TWh	District heating network size local configuration	Section 3.2 for more details
Fav.Expan, *Ch.Expan*, *Ch.Effi*, *Con.Effi*	Prospective scenarios for heat demand evolution and electricity prices	
Geo, Bio	Initial heat production mix configurations	
Geo20, Geo40, Bio20, Bio40	Initial heat production mix and HTN length configurations	

Table 5: Acronyms

Notation	Description	Unit
	Indices and superscripts	
$y \in \mathscr{Y}$	Year block starting with year y	
$t \in \mathscr{T}$	Hours	
$k \in \mathscr{K}$	Alternative heat production capacity	
$i \in \mathscr{I}$	Pipe number	
$j \in \mathscr{J}$	Pipe combination number	
ext	Heat extraction system	
$capa$	Alternative heat production capacities	
$pump$	Pumping stations	
	Variables	
$K^{capa,new}_{k,y}$	capacity of AHPC k added or decommisioned at the beginning of year block y	[MW]
$\mathbf{I}^{pipe}_{i,y}$	indicator function of pipe i being built at the beginning of year block y	
$K^{<comp>}$	capacity of component <comp>	[MW]
$K^{pump,new}_{y}$	pumping power capacity added or decommissioned at the beginning of year block y	[MW]
$q^{capa}_{k,t'}$	hourly heat production of alternative heat production capacity k	[MWh]
$\mathbf{I}^{act}_{k,t'}$	indicator function of AHPC k being a.	
$q^{ext}_{t'}$	hourly quantity of heat extracted from the secondary circuit of the NPP	[MWh]
$q^{supp}_{t'}$	hourly quantity of heat supplied from the heat transmission network to the DH network	[MWh]
$P^{SG}_{t'}$	Steam generator power	[MW]
$P^{e}_{t'}$	Electrical power of the NCP	[MW]
$\dot{m}^{ext}_{t'}$	Total mass flow rate extracted by the heat extraction module	[kg/s]
$\Delta\dot{m}^{HP}_{t'}$	Mass flow rate extracted at the inlet of the high pressure turbine	[kg/s]
$\Delta\dot{m}^{LP}_{t'}$	Mass flow rate extracted at the inlet of the low pressure turbine	[kg/s]
$\Delta\dot{m}^{cond}_{t'}$	Mass flow rate extracted at the inlet of the condenser	[kg/s]
$\Delta P^{e}_{t'}$	hourly power generation loss	[MWh_e]
$IC^{<comp>}_{y}$	installation cost of component $< comp >$ at year y	[€]
$FOM^{<comp>}_{y}$	annual fixed O&M cost of component $< comp >$	[€]
$VO^{<comp>}_{t'}$	hourly variable operation cost of component $< comp >$	[€]
$OC_{t'}$	opportunity cost of loss of electric power due to steam extraction	[€]
$\mathbf{U}^{comb}_{j,t'}$	indicator function of pipe combination j being used	
$\mathbf{A}^{pipe}_{i,y}$	indicator function of pipe i being available during year block y	
$\mathbf{A}^{comb}_{j,y}$	indicator function of pipes combination j being available during year block y	

Table 6: Indices and variables of the model

Notation	Description	Unit
β	Discount factor	
$q_{t'}^{dem}$	Net hourly heat demand	[MWh]
E_y^{max}	GHG intensity cap	[tCO_2eq/MWh]
$\overline{K}_k^{capa}$	Maximum capacity of AHPC k that can be installed	[MW]
$\overline{K_k^{capa,new}}$	Maximum capacity of AHPC k that can be installed each year block	[MW]
$q_{min,k}^{capa}$	Minimum load of AHPC k when it is turned on	[MW]
τ_k	Maximum ramping rate of capacity k	[%]
τ_{SG}	Maximum ramping rate of the steam generator	[%]
τ_{BoP}	Maximum rate of change of the BoP dispatch	[%]
η_{ran}	Efficiency of the Rankine cycle of the reactor	
P_{nom}^{SG}	nominal power of the steam generator	
P_{max}^{sg}	Maximum steam generator heat production rate	[MW]
γ_e	Minimum electricity production fraction	[%]
γ_{SG}	Minimum steam generator power fraction	[%]
$c_y^{<comp>,inst}$	Installation cost of component at year y per unit of capacity	[€/MW]
$c_{k,y}^{capa,inst}$	Installation cost of AHPC k at year y per unit of capacity	[€/MW]
$c_i^{pipe,inst}$	Installation cost of pipe i	[€]
$c^{ext,fom}$	Annual specific fixed O&M cost of the heat extraction system	[€/MW/yr]
$c_i^{pipe,fom}$	Fixed O&M cost of pipe i	[€/yr]
$c^{pump,fom}$	Annual specific fixed O&M cost of pumping stations	[€/MW/yr]
$c_{k,y}^{capa,fom}$	Annual fixed O&M cost of AHPC k at year y per unit of capacity	[€/MW/yr]
$c^{ext,vo}$	Specific variable operation cost of the heat extraction system	[€/MWh]
$c^{capa,vo}$	Specific variable operation cost of AHPC k	[€/MWh]
EF_k^{capa}	Emission factor of capacity k	[tCO_2/MWh]
l_{ext}	Lifetime of the heat extraction system	[years]
l_{pump}	Lifetime of the pumping stations	[years]
l_k	Lifetime of AHPC k	[years]
$p_{y,s,t}^e$	Electricity price (day-ahead price)	[€/MWh]
$p_{k,t'}^{fuel}$	Fuel price for technology k	[€/MWh]
η_k	Conversion efficiency of technology k	[€/MWh]
$p_{t'}^{co2}$	Price of CO_2 emissions	[€/tCO_2]
M_{conv}	Conversion matrix between pipes availability and pipe combinations availability	
f_j^{pump}	Pumping power approached function for combination j	
f_j^{ext}	Heat load extraction approached function for combination j	
$f_j^{\dot{m}}$	Mass flow extraction approached function for combination j	
$\overline{\theta}_j$, $\underline{\theta}_j$	Regression coefficients for HTN feasible operating regions	
T_{ext}	Temperature supplied by the heat extraction module to the HTN	°K
T_{HP}	Temperature at the inlet of the high pressure turbine	°K
T_{LP}	Temperature at the inlet of the low pressure turbine	°K
T_{cond}	Temperature at the inlet of the condenser	°K
$\dot{m}_{nom}^{HP}$	Steam flow at the inlet of the high pressure turbine in nominal operation	[kg/s]
$\dot{m}_{nom}^{LP}$	Steam flow at the inlet of the low pressure turbine in nominal operation	[kg/s]
L	Length of each of the supply and return pipes	[m]
D_i	Diameter of pipe i	[m]
η_{pump}	Efficiency of the pumping stations	
$\alpha_j^{pump,m}$, $\alpha_j^{pump,q}$, ...	Polynomial regression coefficients for w^{pump}	
$\alpha_j^{heat,m}$, $\alpha_j^{heat,q}$, ...	Polynomial regression coefficients for q^{supp}	

Table 7: Parameters of the model

6.2 Heat demand pattern

The heat demand pattern considered in the paper is built with the model proposed by (Ruhnau et al., 2019). The hourly demand is built by multiplying a hourly profile factors to a the daily demand. For a given day, average daily heat demand is computed based on a weighted average of effective exterior temperatures of the four days preceding the day of interest.

The hourly shape factor applied to a DH demand depends on the type of buildings fueled by the DH network. The German Association of Energy and Water Industries (BDEW) provides data to compute these hourly shape factors for all types of buildings, and proposes to average the building-specific curves (weighted by their share in the DH consumption). These data are made available in the BDEW report untitled "Guidelines for the processing of standard gas load profiles", published in 2016.[18]

We apply this methodology on 2019 Paris' weather data to get our hourly heat demand profile. The demand profile is then scaled to meet the annual total heat demand of each scenario studied.

6.3 Technical and economic parameters data

Table 8: Cost parameters for alternative heat production capacities

Technology	Fuel	VO (€/MWh)*	FOM (€/kW/yr)	IC (€/kW)	Source
Heat pumps	Electricity	0.5	30	1500	(a)(b)
Solid Biomass	Biomass	5.4	16	800	(a)
Gas burners	Natural Gas	3	4	– **	(c)
Geothermal	Electricity	0.5	40	2000	(a)(d)
SWI***	Solid Wastes	0	0	0	–

* excluding fuel cost
** Discarded as the model is not allowed to invest in NG boilers
*** Solid Waste Incineration provides a service to the municipality (getting rid of wastes), therefore it is assumed as having 0 cost and unlimited lifetime
(a) (Pursiheimo et al., 2022), (b) (Pavičević et al., 2017), (c) (Lavialle et al., 2023), (d) (Fridleifsson, 2001)

6.4 Future electricity prices

The electricity prices taken for our analysis is built from 2019 Epex Spot data for France. We have distorted these historical data to obtain hourly price profiles that are more realistic in terms of the evolution of the electricity generation mix in the coming years. Indeed, the development of renewable generation resources, and in particular solar PV, as well as new consumption patterns (e.g. electric cars) will have an impact on electricity prices in their daily shape, which must be taken into account for a reliable analysis.

We use data from Aurora and the EU-SysFlex European Project scenarios to obtain seasonal and hourly deformation factors for each year between 2025 and 2050 that we apply on the historical data.

6.5 Representative weeks selection

The investment phase of our optimization problem relies on the use of representative weeks to model the short-term operation of the NCP, the HTN and the AHPCs. The representative weeks selection algorithm is based on the work of (Helistö et al., 2020). We use a K-means algorithm to obtain N clusters (N=10 in this paper) of sampled weeks. Then, within each cluster, we select the week which has the lowest RMSD with the other samples of the cluster. (Weeks start at 12pm on day d and end at 23pm on day $d+6$.)

[18] See https://www.bdew.de/media/documents/Leitfaden_20160630_Abwicklung-Standardlastprofile-Gas.pdf.

The data on which this selection is done is made of the concatenation of the normalized head demand and normalized electricity price data with an hourly resolution. Therefore, the K-means and minimum RMSD selection is applied on vectors of length 336.

6.6 Model equations

6.6.1 Nuclear cogeneration plant model (linearized)

Equations (35) to (39) model the loss of electric power generation due to the extraction of steam in the secondary circuit.[19]

$$P^{e}_{t'} = \eta_{ran} P^{SG}_{t'} - \Delta P^{e}_{t'} \tag{35}$$

$$P^{e}_{t'} \geq \gamma_{e} \eta_{ran} \cdot P^{SG}_{t'} \tag{36}$$

$$\Delta P^{e}_{t'} = \Delta P^{e,HP}_{t'} + \Delta P^{e,LP}_{t'} \tag{37}$$

$$\Delta P^{e,HP}_{t'} = \Delta \dot{m}^{HP}_{t'} \cdot \frac{P^{e,HP}_{nom}}{\dot{m}^{tot}_{nom}} \tag{38}$$

$$\Delta P^{e,LP}_{t'} = P^{e,LP}_{nom} \cdot \left(\frac{\Delta \dot{m}^{LP}_{t'}}{\dot{m}^{LP}_{nom}} + \frac{\Delta \dot{m}^{HP}_{t'}}{\dot{m}^{tot}_{nom}}\right) \tag{39}$$

Equations (41) and (40) model the mass flow and thermal power balance in the heat extraction module. $MT^{ext}_{t'}$ corresponds to the product of the extracted mass flow rate $\dot{m}^{ext}_{t'}$ and the extraction temperature T^{ext}. This product is treated as a variable in itself.

$$\Delta \dot{m}^{HP}_{t'} + \Delta \dot{m}^{LP}_{t'} + \Delta \dot{m}^{cond}_{t'} = \dot{m}^{ext}_{t'} \tag{40}$$

$$\Delta \dot{m}^{HP}_{t'} \cdot T_{HP} + \Delta \dot{m}^{LP}_{t'} \cdot T_{LP} + \Delta \dot{m}^{cond}_{t'} \cdot T_{cond} = MT^{ext}_{t'} \tag{41}$$

Heat extraction and heat transmission subsystems include non-linear equations that we wish to linearize in the context of this paper. To do so, as a preprocessing step, we explicitly model the physics-based equations of the two subsystems together, and applied a linear regression on their simulation in different operation conditions. These allowed us to obtain an approached linear model of the heat extraction and heat transmission system. The detail of this preprocessing step is given in 6.6.2

The regression of the physics-based model of the heat extraction and the heat transport network submodels provide us with the relationship between the heat supplied to the DH network (q^{supp}) and the mass flow extracted from the secondary circuit ($\dot{m}^{ext}$), given in Equation (42). The calculation of the extracted heat from the regressed submodel is given in (43), and the limitation of this extracted amount of heat by the capacity of the heat extraction module is given in (45). Finally, Equation (44) provides the relationship between MT^{ext} and the heta supplied.

$$\dot{m}^{ext}_{t'} = \sum_{j \in \mathcal{J}} f^{\dot{m}}_{j}(q^{supp}_{t'}) \cdot \mathbf{U}^{comb}_{j,t'} \tag{42}$$

$$q^{ext}_{t'} = \sum_{j \in \mathcal{J}} f^{ext}_{j}(q^{supp}_{t'}) \cdot \mathbf{U}^{comb}_{j,t'} \tag{43}$$

$$MT^{ext}_{t'} = \sum_{j \in \mathcal{J}} f^{MT}_{j}(q^{supp}_{t'}) \cdot \mathbf{U}^{comb}_{j,t'} \tag{44}$$

$$q^{ext}_{t'} \leq K^{ext} \tag{45}$$

[19] γ_e is set to 0 here. This means that we allow the cogeneration plant to produce up to 100% heat and no electricity when required. However, high ratios of heat over electricity cogeneration operation require additional engineering studies to assess their feasibility in terms of safety, and performance of the secondary circuit.

Table 9: Technical parameters for alternative heat production capacities

Technology	Lifetime (yrs)	Ramp (%max rate / minute)	Min rate (% max rate)	Efficiency or COP (%)	Emission factor (tCO_2/MWh)	Source
Heat pumps	25	6	0	280	–*	(a)(b)
Solid Biomass	25	5**	0	77***	0	(a)(c)
Gas burners	30	5	15	90	0.45	(d)
Geothermal	30	6	0	350	–*	(e)
Solid Waste Incineration	– ****	5 **	0	– ****	0	–

* Average european emission factor of electricity production is taken as the emission factor for heat pumps and geothermal capacities (corrected by COP). A linear decrease from 2025 value (0.2 tCO_2/MWh) to zero emissions in 2050 is assumed.
** Assumed similar to NG boilers
*** Median value retained
**** Solid Waste Incineration provides a service to the municipality (getting rid of wastes), therefore it is assumed as having 0 cost and unlimited lifetime

(a) (RTE, 2023) (b) (Meesenburg et al., 2018) (c) (Chau et al., 2009) (d) (Lavialle et al., 2023) (e) (Buonomo et al., 2022)

Table 10: Electricity price scenarios

		Scenarios	
		Low	High
2025	Average Oct→Apr prices (€/MWh)	64	154
	Standard deviation Oct→Apr (€/MWh)	25	43
	Average Apr→Oct prices (€/MWh)	43	120
	Standard deviation Apr→Oct (€/MWh)	27	52
2050	Average Oct→Apr prices (€/MWh)	61	133
	Standard deviation Oct→Apr (€/MWh)	23	65
	Average Apr→Oct prices (€/MWh)	39	59
	Standard deviation Apr→Oct (€/MWh)	15	49

The NCP is also subject to technical constraints regarding maximum heat extraction capacities, minimum steam generator rate, and ramping rates.[20] These constraints are modeled with the following equations:

$$-\tau_{BoP} \cdot K^{ext} \leq q^{ext}_{t'} - q^{ext}_{t'-1} \leq \tau_{BoP} \cdot K^{ext} \quad (46)$$

$$-\tau_{SG} \cdot P^{SG}_{nom} \leq P^{SG}_{t'} - P^{SG}_{t'-1} \leq \tau_{SG} \cdot P^{SG}_{nom} \quad (47)$$

$$P^{SG}_{t'} \geq \gamma_{SG} P^{SG}_{nom} \quad (48)$$

6.6.2 Regression for HTN and heat extraction subsystems

The heat transmission network is subject to heat losses, and pressure losses. The system of equations governing these two phenomenon include non-polynomial equations and third degree polynomial terms, and requires to model the losses in each of the pipes, since the coefficients governing the losses depend on the dimensions of the pipes. As a result, including this exact system in the model would increase a lot the calculation time needed to solve the optimization problem. Therefore, we propose a new method to simplify the heat transmission network sub-system of equations. The proposed methodology described in Figure 18 is composed of four main steps: Selecting pipe combinations we are interested in, computing the operating region in terms of suppliable heat, simulating the operation of the HTN for different values of heat supplied within the feasible range, and fitting quadratic curves to get approached forms of the thermal loss, pressure losses, extracted heat, and extraction mass flow rate. Below we describe in more details each of these steps:

1. We first select the set $\mathscr{J}$ of pipe combinations that the HTN is allowed to use. Using pipe combination j means that the transmission network opens all the pipes (both supply and return) of combination j, and flows water at one unique velocity for the supply pipes, and one unique velocity for the return pipes.

[20] We use $\tau_{BoP} = 1$, $\tau_{SG} = 0.6$, and $\gamma_{SG} = 0.2$

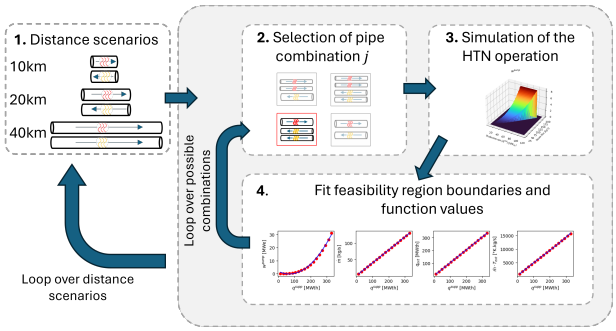

Figure 18: Methodology to simplify the heat transmission network sub-system

2. We then compute the minimum and maximum theoretical heat suppliable through the HTN (without consideration of the extraction limitations from the NCP). This depends only on the maximum velocity reachable in the pipes, and the thermal loss calculation. Therefore, we obtain a pair ($q^{supp}_{min,j}$,$q^{supp}_{max,j}$) for each pipe combination j.

3. Then, the exact system of equations representing the heat extraction and HTN sub-systems are used to simulate the operation of the two coupled systems under given operating conditions. In practice, the input variables are the pipe combination used (j) and the heat supplied to the DH network (outlet side of the HTN). Other input (fixed) parameters include the outlet temperature of the heat extraction module, and the supply and return temperatures on the DH side of the HTN. The output variables of interest are the heat extracted by the heat extraction system and entering the HTN (q^{ext}), the mass flow rate extracted from the secondary circuit $\dot{m}^{ext}$, the mass-temperature flow rate (MT^{ext}), and the pumping power required to compensate for pressure losses in the HTN (w^{pump}). The original equation system representing the operation of the heat transmission network is provided in section 6.6.3. The original equations representing the operation of the heat extraction subsystem is provided in section **??**.

4. Finally, the simulated operating conditions are used to obtain approached quadratic forms for the output variables. The polynomial coefficients are obtained by performing a polynomial regression for each combination j between q^{supp}, and the output variables. Regression coefficients are provided in the Appendix.

   In practice, we only use the linear form (intercept and 1st order coefficients) of these regressed equations, except for the pumping power, for which we use the 2nd order polynomial regres-

sion, and linearize it in our Mixed-Integer Linear Programming problem with Special Ordered Set (SOS) constraints.

6.6.3 Original non-approached heat transmission network subsystem

In this subsection, we describe the equations that govern the operation of the heat transfer network. Variables that depend on time are indexed by t (hours). Our representation of the HTN is inspired by the work of (Hirsch et al., 2018) and (2016). However, there are some differences. For example, we do not discretize the spatial dimension and pumping stations in our problem[21], and we use different constraints for supply and return temperatures as the ones used in (2018).

Pipe characteristics and thermodynamic quantities are also indexed by d, which represents the piping direction (either supply "S", or return "R"). A representation of the HTN is shown on Figure 19. The result of the polynomial regressions performed to simplify the HTN equation system depends on the values of the characteristics of the pipes and pumping stations considered. The notation and values of the thermodynamic and equipment parameters that are used in the HTN equations system are summarized in table 11.

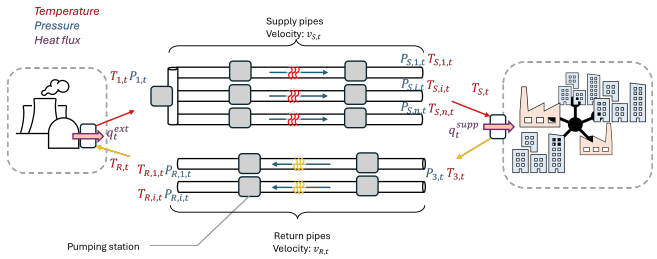

Figure 19: Heat transmission network representation with the associated variables

Pipes areas and friction coefficients are given in Equations (49) and (50)[22].

$$A_{d,i} = \pi(D_{d,i}/2)^2 \tag{49}$$

$$f_{d,i} = 1/\left(4log_{10}(\frac{\xi_{d,i}}{3.7D_{d,i}})^2\right) \tag{50}$$

The water mass flow rate circulating in each pipe is given in Equation (51), and the total water mass flow rate of the system is described in Equation (52) where $\mathbf{U}_{i,t}^{pipe}$ is the indicator function of pipe i being used at time t. Since the HTN is assumed to operate in a closed loop, the water flows in the supply and return systems are equal.

$$\dot{m}_{d,i,t} = \rho A_{d,i} \cdot v_{d,t} \cdot \mathbf{U}_{i,t}^{pipe} \tag{51}$$

$$\dot{m}_t = \sum_i \dot{m}_{d,i,t} \quad \text{, for } d = S \text{ and } d = R \tag{52}$$

Pressure losses and final pressure at the outlet of the supply and return pipes are described in Equations (53) to (59).

$$\Delta P_{d,i,t} = -\frac{\rho f_{d,i} L}{2d_{d,i}} \cdot v_{d,t}^2 \tag{53}$$

$$P_{S,i,t} = P_{1,t} + \Delta P_{S,i,t} + \Delta P_{S,i,t}^{pump} \tag{54}$$

$$P_{R,i,t} = P_{S,t} + \Delta P_{R,i,t} + \Delta P_{R,i,t}^{pump} \tag{55}$$

$$w_t^{pump} = \dot{m}_t/\eta_{pump} \cdot \left(\sum_i \Delta P_{S,i,t}^{pump} + \sum_i \Delta P_{R,i,t}^{pump}\right) \tag{56}$$

$$P_{d,min} \leq P_{d,i,t} \tag{57}$$

$$P_{1,t} = P_1 \text{ (input)} \tag{58}$$

$$P_{S,t} = \frac{\sum_1^{n_S^{pipe}} A_{S,i} \cdot \mathbf{U}_{S,i,t}^{pipe} \cdot P_{S,i,t}}{\sum_1^{n_S^{pipe}} A_{S,i} \cdot \mathbf{U}_{S,i,t}^{pipe}} \tag{59}$$

Finally, thermal losses in the pipes are modeled in Equations (60) to (69).

$$T_{R,t} = \frac{\sum_1^{n_R^{pipe}} A_{R,i} \cdot \mathbf{U}_{R,i,t}^{pipe} \cdot T_{R,i,t}}{\sum_1^{n_R^{pipe}} A_{R,i} \cdot \mathbf{U}_{R,i,t}^{pipe}} \tag{60}$$

$$T_{2,t} = \frac{\sum_1^{n_S^{pipe}} A_{S,i} \cdot \mathbf{U}_{S,i,t}^{pipe} \cdot T_{2,i,t}}{\sum_1^{n_S^{pipe}} A_{S,i} \cdot \mathbf{U}_{S,i,t}^{pipe}} \tag{61}$$

$$T_{3,t} = T_{return} \tag{62}$$

$$T_{S,t} \leq T_{S,min} \tag{63}$$

$$T_{1,t} = T^{ext} \tag{64}$$

$$T_{1,t} = T_{R,t} + \frac{q_t^{ext}}{c_p.\dot{m}_t} \tag{65}$$

$$T_{R,i,t} = \mathbf{Temp}(T_{R,t}, \lambda_{R,i}, \dot{m}_{R,i,t}) \tag{66}$$

$$T_{2,i,t} = \mathbf{Temp}(T_{1,t}, \lambda_{S,i}, \dot{m}_{S,i,t}) \tag{67}$$

$$\mathbf{Temp}(T_i, \lambda, \dot{m}) = (T_i - T_g)\exp(-\frac{\lambda L}{\dot{m}c_p}) + T_g \tag{68}$$

$$q_t^{supp} = (T_{S,t} - T_{3,t}).c_p.\dot{m}_t \tag{69}$$

[21] Because we are not interested in the locations of pumping stations along the HTN path.

[22] See (2018)

Table 11: Parameters for the pipes and thermodynamic equations of the HTN

Parameter	Description	Value	Source
$D_{d,i}$	diameter of pipe i in direction d	0.25m, 0.5m, 0.75m	(Abushamah et al., 2023)
$A_{d,i}$	area of pipe i in direction d	*calculated* [m^2]	-
$f_{d,i}$	friction coefficient of pipe i in direction d	*calculated*	(Hirsch et al., 2018)
$\xi_{d,i}$	roughness of pipe i in direction d	0.1mm	(2018)
$\lambda_{d,i}$	heat loss coefficient of pipe i in direction d	0.02 W/K/m	(2018)
$T_{S,min}$	Minimum supply temperature	120°C	(El Mrabet et al., 2024)
L	Distance	20km and 40km each way	-
ρ	volumetric mass of water (assumed constant),	1 kg/m^3	-
c_p	specific heat capacity of water	4184 J/kg/K	
η_{pump}	Efficiency of the pump	0.75	(Hirsch et al., 2018)
$P_{d,min}$	minimum pressure in the pipes to ensure a proper operation of the HTN	0.2MPa for d=S, 0.05MPa for d=R	(2018)
P_1	Initial pressure for steam extracted	*calculated* [MPa]	-